Targeting PDK and PARP to improve radiation response in preclinical models of non-small cell lung cancer

Tom Verbiest

St Edmund Hall

A thesis submitted to the Division of Medical Sciences at the University of Oxford for the Degree of Master by Research

Trinity Term 2013

Gray Institute for Radiation Oncology and Biology

Department of Oncology

University of Oxford

Word count: 16,046

Abstract

Approximately 50 % of all NSCLC patients receive radiation therapy during the course of their disease, and the quest to enhance the radiation response of these patients is still ongoing. Here, we investigate the potential to increase the radiation response of NSCLC by targeting the PI3K signalling pathway with PDK1 inhibitors and/or targeting DNA repair with the PARP inhibitor olaparib. The *in vitro* radiosensitising effect of the PARP inhibitor olaparib and the PDK1 inhibitors BX912 and GSK2334470 was determined using clonogenic survival assays. The combination of PDK1 inhibitors with radiation did not increase the radiosensitivity of NSCLC cell lines, irrespective of the TP53 status. However, a significant radiosensitisation was observed by addition of olaparib to radiation treatment (SER_{50} 1.6 to 2.2). Immunofluorescent quantification of γH2AX foci formation indicated that the radiosensitisation effect of olaparib could be explained by inhibition of DNA repair. Subsequently, we demonstrated that olaparib enhances the radiosensitivity of a poorly vascularised NSCLC xenograft model by decreasing DNA repair and increasing apoptosis. In contrast, a well vascularised NSCLC model was not sensitised by addition of olaparib to radiation treatment. The effect of olaparib on *in vivo* vascular perfusion was assessed using dynamic contrast enhanced-magnetic resonance imaging. No significant differences were observed between olaparib and vehicle treated xenografts, suggesting that the radiosensitising effect can be mainly attributed to inhibition of DNA repair. We demonstrated that olaparib is a potent radiosensitiser in a poorly vascularised lung cancer model but further *in vivo* experiments are warranted to identify the subset of patients that would benefit from olaparib addition to radiation therapy.

Table of content

List of figures

List of tables

List of abbreviations

ALK	Anaplastic lymphoma kinase
APE1	Apurinic–apyrimidinic endonuclease 1
AT	Ataxia-telangiectasia
CAIX	Carbonic anhydrase IX
CC3	Cleaved Caspase 3
DCE-MRI	Dynamic contrast enhanced-magnetic resonance imaging
DMEM	Dulbeco's modified eagle medium
DMSO	Dimethyl sulfoxide
DSB	Double-strand break
EGFR	Epidermal growth factor receptor
FBS	Foetal bovine serum
GF	Growth factor
HR	Homologous recombination
HRP	Horse radish peroxidase
IP	Intraperitoneal
IR	Ionising radiation
mTORC	Mammalian target of rapamycin complex
NHEJ	Non-homologous end-joining
NSCLC	Non-small cell lung cancer
pAKT	phospho-AKT
PARG	Poly(ADP-ribose) glycohydrolase
PARP	Poly(ADP-ribose) polymerase
PBS	Phosphate buffered saline
PCNA	Proliferating cell nuclear antigen
PDPK1	Phosphoinositide-dependent protein kinase 1
PE	Plating efficiency
PFA	Paraformaldehyde
PFPE	Paraformaldehyde fixed paraffin embedded
PH	Pleckstrin homology

PI3K	Phosphatidylinositol-3-kinase
PIP2	Phosphatidylinositol-4,5-biphosphate
PIP3	Phosphatidylinositol-3,4,5-triphosphate
PNK	Polynucleotide kinase
pPDK1	phospho-PDK1
pS6	phospho-S6
PTEN	Phosphatase and tensin
RT	Room temperature
RTK	Receptor tyrosine kinase
RTV	Relative tumour volume
S6K1	p70S6 kinase 1
SCLC	Small cell lung cancer
SER	Sensitisation enhancement ratio
SF	Surviving fraction
SSB	Single-strand break
SSBR	Single-strand break repair
TBS	Tris buffered saline
TGD	Tumour growth delay
TGT	Tumour growth time
TKI	Tyrosine kinase inhibitor
TMA	Tissue microarray
VEGF	Vascular endothelial growth factor
XRCC1	X-ray repair cross-complementing protein 1

CHAPTER 1

Introduction

1. Introduction

1.1. Lung Cancer

Lung cancer is the most common cancer diagnosed worldwide and accounts for approximately 1.4 million cancer deaths each year (Ferlay, Shin et al. 2010). Of all lung cancer patients, 15 % are diagnosed with small cell lung cancer (SCLC) and 85 % with non-small cell lung cancer (NSCLC) (Herbst, Heymach et al. 2008). NSCLC can be further subdivided into three major histologic subtypes: adenocarcinoma, squamous cell carcinoma and large cell carcinoma (40.8 %, 21.4 %, and 2.6 % of all lung cancers, respectively) (Howlader, Noone et al. 2013). Whereas a decline in lung cancer incidence in men has been observed since the late 1980s, the lung cancer incidence in women has not decreased and is even expected to increase in the forthcoming years (Malvezzi, Bertuccio et al. 2013).

Despite significant progress in early detection, and recent advances in chemotherapy, radiotherapy and targeted therapies, the 5-year survival for lung cancer patients remains the second lowest of the twenty most common cancers diagnosed in the United Kingdom (only pancreatic cancer has a lower survival rate). The overall 5-year survival for British men diagnosed with lung cancer has increased over the past 40 years only from 4 % to 7.8 %, and for women from 4 % to 9.3 %. In general, lung cancer patients still have a very poor prognosis, due in part to the majority of patients (68 %) presenting with locally-advanced (32%) or advanced stage lung cancer (36%), a stage at which palliative treatment represents the standard of care (Bareschino, Schettino et al. 2011; Cancer Research UK 2012) .

1.2. Conventional NSCLC Therapies

Lung cancer treatment strategy is mainly determined by the stage of disease at the time of diagnosis. Stage I and II NSCLC, often referred to as localised disease, are primarily managed by surgical resection, with 5-year survivals of 35 % and 21 %, respectively. Patients with localised disease but positive surgical margins may benefit from postoperative radiotherapy, and patients with stage II disease may additionally benefit from adjuvant chemotherapy. For stage III NSCLC, in which the tumour has spread beyond the nearby lymph nodes but not beyond the thoracic cavity, a combination of definitive thoracic radiation and chemotherapy is the cornerstone of treatment but is only modestly effective despite high toxicity (5-year survival of 6%) (Ihde and Minna 1991; Cancer Research UK 2012). Stage IV NSCLC, in which metastases are present beyond the thoracic cavity, has only anecdotal 5-year survival, and chemotherapy or radiotherapy are offered with palliative intent (Lally, Zelterman et al. 2006; Cancer Research UK 2012; Saintigny and Burger 2012).

Overall, approximately 50 % of all NSCLC patients will receive radiation therapy at some time during the course of their disease. Radiotherapy is used as an alternative to surgery in early stage (stage I/II) cancer for patients who are not suitable candidates for surgery, as a single agent or in combination with chemotherapy in stage III (locally-advanced) cancer and as palliation of symptoms in stage IV cancer. Patients presenting with brain metastasis receive radiotherapy as palliation or increasingly as potential curative for isolated metastases where no evidence of other systemic disease has been identified (Barbera, Zhang-Salomons et al. 2003).

Genetic alterations in NSCLC, such as activating point mutations in the epidermal growth factor receptor (EGFR) gene and rearrangement of the anaplastic lymphoma kinase (ALK) gene (most commonly to produce an EML4-ALK fusion protein), now define specific molecular cohorts of patients that can be treated with targeted therapies, such as tyrosine kinase inhibitors (TKIs) and monoclonal antibodies. Receptor tyrosine kinases (RTKs) consist of an extracellular domain containing the ligand-binding site, a transmembrane α helix, and a cytosolic domain which contains the protein-tyrosine kinase activity. Binding of the ligand causes the RTK to dimerise**.** The protein kinase of the receptor monomer then phosphorylates a set of tyrosine residues of the dimer partner. Initially, the tyrosine residues in the catalytic site become phosphorylated, leading to a conformational change which facilitates binding of ATP and protein substrates. Then the RTK phosphorylates other sites in its cytosolic domain. This autophosphorylation results in the phosphotyrosine residues serving as docking sites for proteins involved in the downstream signalling, such as PI3K (Hennessy, Smith et al. 2005).

Multiple TKIs have been approved for treatment of NSCLC. Gefitinib and erlotinib inhibit EGFR tyrosine kinase, thereby reducing tumour cell proliferation and anti-apoptotic signalling (Sordella, Bell et al. 2004). Crizotinib inhibits constitutively active ALK activity (as in the EML4-ALK fusion protein), resulting in induction of apoptosis and inhibition of tumour cell proliferation (McDermott, Iafrate et al. 2008). The next generation TKI afatinib irreversibly inhibits human EGFR family members and has recently been approved as first-line treatment for metastatic non-small cell lung cancer with common EGFR mutations (Boehringer Ingelheim Pharmaceuticals 2013).

The monoclonal antibody bevacizumab, registered for use in addition to platinum-based chemotherapy for first-line treatment of unresectable advanced, metastatic or recurrent non-small cell lung cancer other than predominantly squamous cell histology, binds vascular endothelial growth factor (VEGF), thereby inhibiting VEGF-dependent angiogenesis, one of the hallmarks of cancer (Sandler, Gray et al. 2006).

1.3. PI3K Signalling in Lung Cancer

1.3.1. PI3K-AKT-mTOR signalling pathway

The phosphatidylinositol-3-kinase (PI3K)/AKT/mTOR signalling pathway plays an important role in cell survival, growth and metabolism, and is activated by binding of growth factors (GF) to RTKs, thereby activating PI3K (cfr supra).

Three distinct PI3K classes have been identified. Class IA PI3Ks consist of heterodimers: a p85 and p110 subunit (ie regulatory and catalytic subunit, respectively). The Src homology-2 domain of the p85 subunit binds to the phosphotyrosine residues in the cytoplasmic domain of activated RTKs. Three isoforms of Class IA p110 have been identified: p110α, p110β and p110δ. Each of the three p85 isoforms (p85α, p85β and p55γ) can bind the p110 isoforms. Class IB PI3Ks consist of a regulatory subunit (p101) and the subunit p110γ. Class II PI3Ks are monomeric and use phosphatidylinositol and phosphatidylinositol-4-phosphate as substrates. Three class II isoforms were identified: PI3K-C2α, PI3K-C2β, and PI3K-C2γ. Class III PI3Ks are heterodimers consisting of a p150 and Vps34 subunit (ie adaptor and catalytic subunit, respectively) (Hennessy, Smith et al. 2005).

Activated class I PI3K phosphorylates phosphatidylinositol-4,5-biphosphate (PIP2), resulting in the formation of phosphatidylinositol-3,4,5-triphosphate (PIP3). An antagonist of PI3K activity, the phosphatase and tensin homolog (PTEN) protein, dephosphorylates PIP3 to produce PIP2 (Cantley 2002). PIP3 recruits and colocalises phosphoinositide-dependent protein kinase (PDPK1, commonly referred to as PDK1) and AKT to the plasma membrane through binding to pleckstrin homology (PH) domain regions in the proteins. Complete AKT activation is achieved through phosphorylation of its threonine 308 residue (Thr308) by activated PDK1, and through phosphorylation of its serine 473 residue (Ser473) by mammalian target of rapamycin complex 2 (mTORC2) (Currie, Walker et al. 1999). Activated AKT stimulates cell growth, survival and metabolism through various mechanisms. It promotes cell survival by inhibiting the proapoptotic proteins BAD and BAX, and also stimulates the mammalian target of rapamycin complex 1 (mTORC1). Activated mTORC1 phosphorylates p70S6 kinase (S6K1), thereby increasing protein synthesis (Cantley 2002).

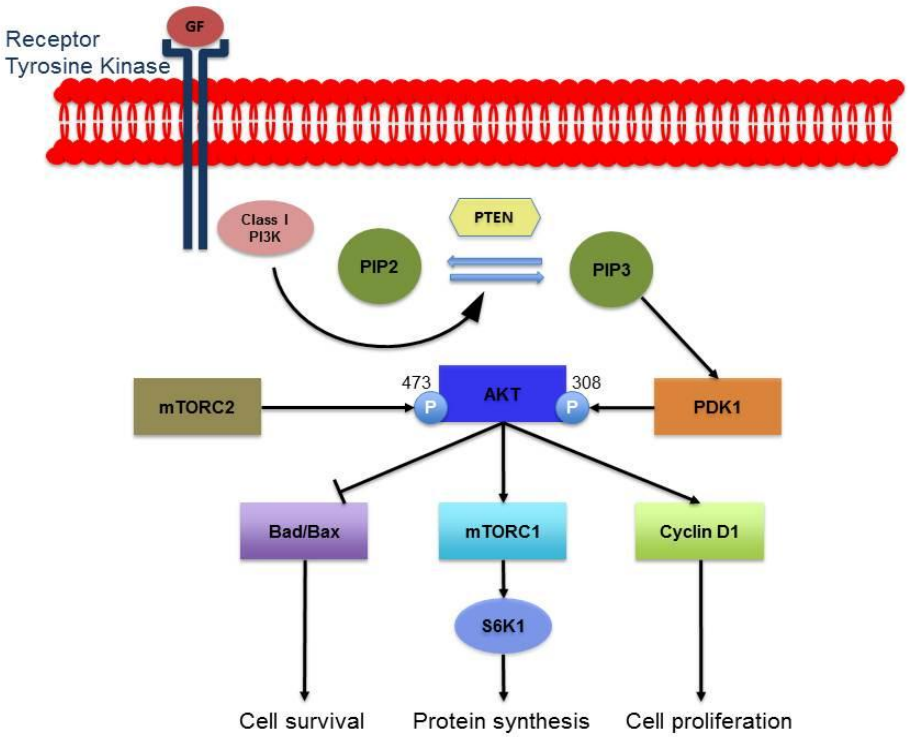

Figure 1.1 PI3K/AKT/mTOR signalling pathway

1.3.2. Activation of the PI3K pathway

Genetic alterations in the components of the PI3K/AKT/mTOR pathway, such as amplification/mutations of RTKs, mutational activation of the *PIK3CA* gene (3 % of NSCLC), amplification of PI3K (66 % of lung squamous cell carcinoma), loss or inactivation of PTEN and overactivation of AKT, significantly increase downstream signalling, thereby promoting cellular survival (Brognard, Clark et al. 2001; Bamford, Dawson et al. 2004; Yamamoto, Shigematsu et al. 2008; Yuan and Cantley 2008). Therefore, pharmacological inhibition of the PI3K pathway is considered an important target for cancer therapy.

1.3.3. Inhibition of the PI3K/AKT/mTOR pathway

Numerous downstream components of the PI3K signalling pathway have been targeted with small molecule inhibitors in cancer treatment. Preclinical data shows that the PI3K inhibitor wortmannin, the mTOR inhibitor rapamycin and the dual PI3K/mTOR inhibitor BEZ235 dose-dependently increase radiosensitivity of NSCLC cells *in vitro* (Konstantinidou, Bey et al. 2009; Nagata, Takahashi et al. 2010; Zhang, Cui et al. 2010).

Four different categories of PI3K pathway inhibitors have reached clinical trials for the treatment of lung cancer (either as monotherapy or combined with conventional therapies): PI3K inhibitors, AKT inhibitors, mTOR inhibitors and dual PI3K-mTOR inhibitors. Currently, PI3K pathway inhibitors are tested in over 20 clinical trials worldwide but to date, no combination studies with radiation therapy have been initiated (World Health Organization 2013).

PDK1 is a key downstream regulator of PI3K signalling, thereby playing a pivotal role in cell survival and proliferation. In addition to activating AKT, PDK1 has other direct downstream targets including S6K1, SGK, RSK and PKC suggesting that inhibition of PDK1 by small molecule inhibitors may have broader effects than inhibiting AKT alone (Najafov, Sommer et al. 2011; Raimondi and Falasca 2011).

In 2005, the first potent submicromolar PDK1 inhibitors, BX912, BX795 and BX320, were reported by Berlex Biosciences (Feldman, Wu et al. 2005). Subsequent experimental studies revealed that these compounds were lacking specificity [other kinases, such as Aurora B and CDK1 were inhibited more potently (Bain, Plater et al. 2007; Tamguney, Zhang et al. 2008)]. It was not until 2011 that three potent and highly selective submicromolar small molecule inhibitors of PDK1 were disclosed [GlaxoSmithKline (Medina, Becker et al. 2011), Pfizer (Murphy, Alton et al. 2011) and Sunesis (Erlanson, Arndt et al. 2011)]. To date, the effect of PDK1 inhibition on radiosensitivity has not yet been reported and none of the PDK1 inhibitors have entered clinical trials (World Health Organization 2013).

1.4. DNA Repair in Lung Cancer

1.4.1. DNA damage detection and repair

Thousands of DNA lesions occur daily in each cell throughout the body (Billen 1990). While some arise through exogenous causes (e.g. ultraviolet radiation and X-rays), other lesions arise through by-products of cellular metabolism (e.g. reactive oxygen species). The majority of the lesions are repaired by specialised DNA repair pathways, present in most mammalian cells (Norbury and Hickson 2001). This section will focus on DNA damage and repair induced by ionising radiation (IR).

An absorbed dose of 1 Gy radiation (such as X-rays) generates approximately 1,000 DNA single-strand breaks (SSBs) and 40 DNA double-strand breaks (DSBs) per cell but the majority of cells will survive demonstrating proficient DNA damage repair pathways are present in mammalian cells (Goodhead 1994; Hall and Giaccia 2006). Depending on the type of damage present in the cell, one or more of the four main DNA repair pathways is activated. Base damage and SSBs are repaired by *base excision repair/single strand break repair* and bulky adducts are removed by *nucleotide excision repair*. *Mismatch repair* removes base-base mismatches and small insertions. DSBs are repaired by either *homologous recombination* (HR) or *non-homologous end-joining* (NHEJ), depending on the phase of the cell cycle (Hoeijmakers 2001). Various DNA repair deficiency disorders, harbouring mutations in the components of the DNA damage response, have been described. For instance, the ataxia-telangiectasia (AT) syndrome is the result of a mutation in the ATM gene and AT patients exhibit, apart from progressive cerebellar ataxia, hypersensitivity to IR (Taylor, Harnden et al. 1975).

The most common type of lesions induced by IR is DNA SSBs (ratio of 25 SSBs to 1 DSB) and these breaks are repaired by the single-strand break repair pathway (SSBR, Figure 1.2). This pathway comprises four basic steps: SSB detection, DNA end processing, DNA gap filling and DNA ligation (Caldecott 2003). The SSB is detected by poly(ADP-ribose) polymerase 1 [PARP1; and PARP2 to a lesser extent], which is activated after binding to the break. Activated PARP uses NAD^+ for the synthesis of branched polymers of ADP-ribose, hereby modifying itself and several acceptor proteins, such as DNA polymerases and topoisomerases (D'Amours, Desnoyers et al. 1999; Herceg and Wang 2001). After recruiting the X-ray repair cross-complementing protein 1 (XRCC1)/DNA ligase 3 complex to the damaged site, PARP is detached and the complex forms a molecular scaffold. PARP also relaxes the chromatin structure to allow access of repair proteins to the damaged site (de Murcia and Menissier de Murcia 1994).

Poly(ADP-ribose)glycohydrolase (PARG) restores PARP to its pre-activated state, thereby preparing the cell for residual SSB detection (Davidovic, Vodenicharov et al. 2001). Following detection, the SSB undergoes end processing. Damaged termini are repaired by apurinic–apyrimidinic endonuclease 1 (APE1) and polynucleotide kinase (PNK). Once the ends are processed, the DNA break undergoes gap filling by short or long patch repair. DNA ligation, the final step in the SSBR pathway, is performed by DNA ligase 1 in short patch repair and by DNA ligase 3 in long patch repair (Caldecott, Tucker et al. 1995; Whitehouse, Taylor et al. 2001).

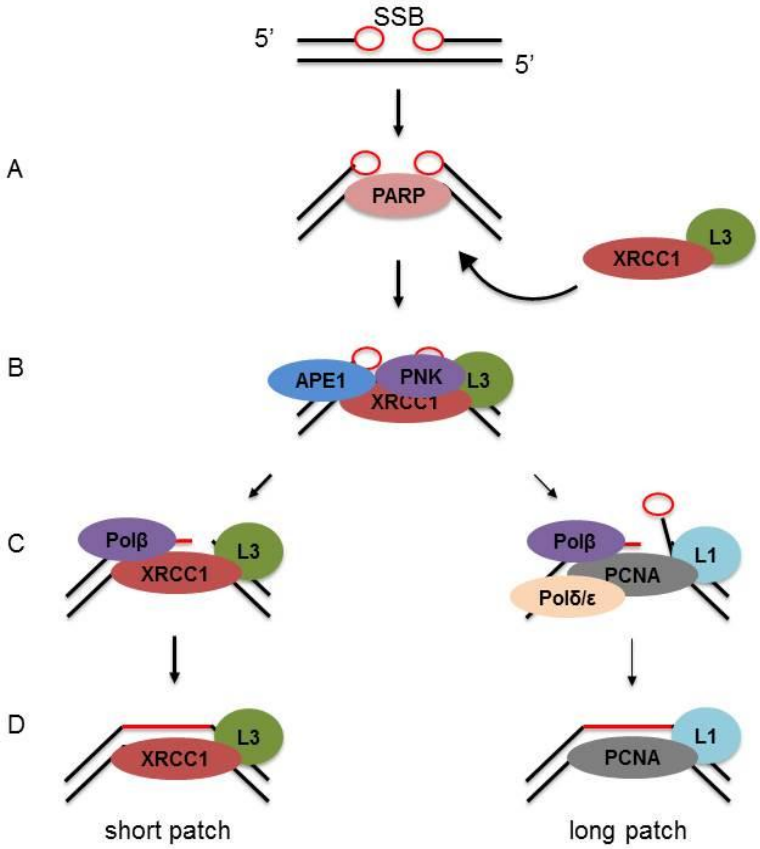

Figure 1.2 Single strand break repair pathway

An overview of the 4 basic steps with (A) SSB detection, (B) end processing, (C) gap filling, and (D) DNA ligation.

The most critical DNA breaks are thought to be those arising in both DNA strands and they can be repaired by two different repair pathways: HR, which uses an undamaged DNA strand as template (error free), and NHEJ, which mediates end-to-end joining (error prone). In human cells, NHEJ is the primary method of DNA DSB repair in all stages of the cell cycle, but cells in the late S/G2 phase of the cell cycle have the additional option of HR which has increased repair fidelity. During the G1 phase of the cell cycle, when no such repair template is present, cells rely on error-prone NHEJ to repair DSBs (Hoeijmakers 2001).

1.4.2. Inhibition of SSB repair by PARP inhibitors

Each year two million fractions of radiotherapy are administered throughout the UK (Powell, Mikropoulos et al. 2010). Although often applied with curative intent, cure rates remain suboptimal. Therefore, a high unmet medical need remains for new therapies to increase the overall radiation response. The tumour radiocurability is governed by 5 different factors, often referred to as the '5 Rs of radiobiology': *repair* of sublethal DNA damage, *redistribution* of cells throughout the cell cycle, *repopulation* by surviving cells, *reoxygenation* between the different fractions of radiation, and the inherent *radiosensitivity* of the cells. Where enhanced repair and repopulation would result in a higher radioresistance; redistribution and reoxygenation enhance the radiosensitivity (Steel, McMillan et al. 1989).

In this section, we will focus on therapeutic agents which impair the DNA repair after radiation therapy, and more specifically, the pharmacological inhibitors of PARP. Although PARP inhibitors were originally developed as chemo- and radiosensitisers (see below), they also gained significant interest within the scientific community by the finding of extreme sensitivity of BRCA1 and BRCA2 deficient breast cancer cells to PARP inhibition (Farmer, McCabe et al. 2005). The breast cancer susceptibility proteins BRCA1 and BRCA2 play a pivotal role in repairing DSBs by homologous recombination. BRCA deficient cells rely more on error prone non-homologous recombination pathways, thereby compromising the genomic integrity of the cell (Tutt, Bertwistle et al. 2001). PARP inhibitors prevent the SSB repair, thereby leading to a stalled replication fork during S phase, and eventually resulting in the formation of lethal DSBs (Kuzminov 2001).

As BRCA deficient cells are deficient in HR, they rely on error prone NHEJ to repair the DNA DSBs which eventually results in genetic instability and cell death (Farmer, McCabe et al. 2005). PARP inhibitors have also been shown to be a useful therapeutic strategy in tumour cells deficient in other components of HR, including ATM and ATR. These phenotypic traits, similar to BRCA deficient cells, are sometimes referred to as 'BRCAness' (McCabe, Turner et al. 2006).

The rationale for PARP inhibition as a potential chemo- and radiosensitiser was set by the *in vitro* observation of compromised DNA repair and enhanced cytotoxicity by radiation and monofunctional alkylating agents in the presence of the nicotinamide analogue 3-aminobenzamide, a first generation PARP inhibitor (Durkacz, Irwin et al. 1981; Thraves, Mossman et al. 1986). These first generation inhibitors lacked specificity and potency (Milam, Thomas et al. 1986). Depletion of PARP activity by an antisense RNA construct was shown to enhance cytotoxicity by alkylating agents in HeLa cells (Ding and Smulson 1994) and an increased radiosensitivity and high genomic instability of PARP knockout mice following radiotherapy and alkylating agents was reported (de Murcia, Niedergang et al. 1997). The second generation inhibitors were developed through screening nicotinamide-resembling compounds, and more potent and specific inhibitors were identified: pthalazinones [olaparib (Cockcroft, Dillon et al. 2006)] and ideno(1,2-c) isoquinolinones [INO-1001 (Jagtap, Baloglu et al. 2005)]. Third generation PARP inhibitors include the benzamidazoles [ABT-888 (Donawho, Luo et al. 2007)] and tricyclic indoles [AGD014699 (Thomas, Calabrese et al. 2007)].

PARP inhibition prevents the automodification of PARP, thereby inhibiting its release from the DNA damage site, eventually preventing access of DNA repair proteins to the SSB. Since PARP is only activated in the presence of DNA SSBs, it was hypothesised that PARP inhibition would act selectively in cells exposed to DNA damaging agents, such as radiation therapy, and would not affect the non-irradiated tissues (Powell, Mikropoulos et al. 2010). Long-term PARP inhibition should be considered carefully though as an accumulation of γH2AX (a marker of potential DNA damage) was observed in eye-brow hair follicles of patients in a phase I trial with the PARP inhibitor olaparib (Fong, Boss et al. 2009).

Abundant pre-clinical data is available demonstrating *in vitro* and *in vivo* chemo- and radiopotentiation by PARP inhibitors. Chemosensitisation has been reported for alkylating agents (Delaney, Wang et al. 2000; Miknyoczki, Jones-Bolin et al. 2003; Calabrese, Almassy et al. 2004; Donawho, Luo et al. 2007; Thomas, Calabrese et al. 2007), topoisomerase inhibitors (Delaney, Wang et al. 2000; Thomas, Calabrese et al. 2007) and anthracyclines (Mason, Valdecanas et al. 2008) in a variety of tumour cell lines and subcutaneous tumour xenografts, including lung, breast and ovarian cancer. Radiosensitisation by PARP inhibitors was reported in a variety of tumour cell lines and subcutaneous xenografts, including lung, colorectal and head and neck cancer (Veuger, Curtin et al. 2003; Calabrese, Almassy et al. 2004; Chalmers 2004; Thomas, Calabrese et al. 2007; Liu, Coackley et al. 2008). Radiosensitisation by ABT-888 was reported to occur under both normoxic and hypoxic conditions (Liu, Coackley et al. 2008).

In previous studies, NSCLC xenograft models have been radiosensitised by PARP inhibition: addition of ABT-888 to radiotherapy was shown to induce a 2-fold increase in tumour growth delay, compared with radiotherapy alone. It was also reported that this combination treatment showed decreased tumour vascular density and cell proliferation on histology, compared with radiotherapy alone (Albert, Cao et al. 2007). Addition of olaparib to radiotherapy induced a 1.4-fold increase in tumour growth delay, compared with radiotherapy alone. It also increased the vascular perfusion in a dorsal window chamber model (Senra, Telfer et al. 2011).

Vasoactive effects, and resulting increased tumour perfusion, have been reported for several PARP inhibitors, including olaparib and AG014699. This increased perfusion was hypothesised to improve drug delivery and oxygenation, thereby contributing to the chemo- and radiosensitising effects of PARP inhibitors (Calabrese, Almassy et al. 2004; Ali, Telfer et al. 2009; Senra, Telfer et al. 2011). To date, it has not been reported whether vascular changes in tumours of cancer patients play a role in the tumour response to PARP inhibitors.

Olaparib is a potent inhibitor of PARP1 and PARP2 [$IC_{50} \leq 2$ nM (Sandhu, Yap et al. 2010)]. In a phase I trial, it was well tolerated up to doses of 400 mg twice daily. Pharmacodynamics demonstrated significant PARP inhibition (> 90 %) from doses of 60 mg (Fong, Boss et al. 2009). Phase II trials in BRCA deficient breast and ovarian cancer confirmed the therapeutic efficacy of PARP inhibition in BRCA mutated cancers (Tutt, Robson et al. 2009; Audeh, Penson et al. 2009). Recently, olaparib entered a phase III trial in ovarian cancer. Currently, four clinical trials investigate olaparib in lung cancer (Table 1.1).

Table 1.1 Ongoing clinical trials investigating olaparib in lung cancer

Most recent data can be found on the 'International Clinical Trial Research Platform' of the World Health Organization.

	Main objective	Phase
A	Olaparib dose escalating in patients treated with radiation therapy with or without daily dose cisplatin for locally advanced NSCLC	I
B	Evaluate the efficacy and tolerability of gefitinib in combination with olaparib versus gefitinib alone, in patients with EGFR mutation positive advanced NSCLC	I/II
C	Establish whether treatment with olaparib in NSCLC which has already responded to induction chemotherapy, delays disease progression compared with placebo	II
D	Olaparib as maintenance programme in small cell lung cancer	II

1.5. Interaction between the PI3K Pathway and PARP

A previous study suggested an interaction between PARP and AKT signalling. It was reported that exposure of the human hepatic cell line WRL-68 to the PARP inhibitor PJ-34 upregulates pAKT levels, thereby increasing anti-apoptotic signalling. Inhibition of pAKT upregulation by the PI3K inhibitor LY294002 counteracted the cytoprotective signalling of the PARP inhibitor (Tapodi, Debreceni et al. 2005). These data suggest that increased AKT signalling following PARP inhibition may provide an increased survival signal, thereby potentially reducing the cytotoxic effects of PARP inhibition either alone or in combination with other cytotoxic agents.

1.6. Aims of the thesis

The overall intent of this thesis was to examine the potential of novel molecularly targeted therapies to augment the radiation response in non-small cell lung cancer. The specific aims of this project were to:

- evaluate the effectiveness of PDK inhibition as a potential radiosensitisation strategy in NSCLC,
- assess whether PDK inhibition could augment olaparib-induced radiosensitisation,
- investigate the *in vivo* effects of olaparib in NSCLC tumour xenografts, both alone and in combination with radiation,
- determine whether the vascular effects of olaparib are detectable in NSCLC tumours using a clinically applicable imaging technique (Gd-enhanced DCE-MRI).

CHAPTER 2

Material and methods

2. Materials and methods

2.1. Mammalian Cell Culture

Human non-small cell lung cancer (NSCLC) cell lines used in this study were obtained from American Type Culture Collection (Table 2.1).

Table 2.1 Human NSCLC cell lines used in the experimental studies
Details on tissue of origin and isolation of the five NSCLC cell lines.

Cell line	Tissue of origin	Isolation
A549	Lung carcinoma	Cell line isolated from 58 year-old Caucasian male in 1972
Calu-3	Lung adenocarcinoma	Cell line isolated from 25 year-old Caucasian male
Calu-6	Lung anaplastic carcinoma	Cell line isolated from 61 year-old Caucasian female in 1976
H1299	Lung carcinoma	Cell line isolated from 43 year-old Caucasian male
H1975	Lung adenocarcinoma	Cell line isolated from female in 1988

Cells were cultured in 75 cm^2 tissue culture flasks (Corning Incorporated, Corning, USA) and incubated in standard culture conditions (37 °C in a 95 % O_2 and 5 % CO_2 environment). Cells were cultured in Advanced Dulbecco's modified eagle medium (DMEM)/F12 (1:1) supplemented with 5 % Foetal Bovine Serum (FBS; Sigma-Aldrich, Dorset, UK), 2 mM Glutamax and 50 µg/mL Penicillin/Streptomycin. All cell culture reagents were purchased from Gibco by Life Technologies (Paisley, UK), unless otherwise stated. The cell lines Calu-3 and Calu-6 were transduced with a lentivector (LVP323, AMS Biotechnology Ltd, Abingdon, UK) containing the luciferase gene and selection was achieved by addition of 10 µg/mL blasticidin S (InvivoGen, San Diego, USA) to the culture medium.

Cells were counted and viability determined using a Neubauer haemocytometer (Paul Marienfeld, Lauda-Königshofen, Germany). Equal volumes of 0.4 % trypan blue (Gibco) and cell suspension were mixed. A volume of 10 µl of the mixture was transferred under the glass cover-slip of the haemocytometer and living cells were counted.

2.2. Western Blot

2.2.1. Sample preparation, electrophoresis and protein transfer

Cells were seeded at 1 x 10^6 cells/well in 6-well plates (Corning Incorporated) and treated the following day. At the experimental endpoint, the plates were washed twice with ice-cold 1x PBS, on ice. Complete lysis buffer was prepared by addition of Na_3VO_4 (Sigma Aldrich) and protease inhibitor (Complete Protease Inhibitor Cocktail; Roche, Welwyn Garden City, UK) to lysis stock buffer (Table 2.2 for lysis stock buffer components).

Cells were lysed with 100 µl of complete lysis buffer for 10 min. Following sonication for 10 seconds at room temperature (RT; Ultrasonic Homogonizer 300 V/T; BioLogics, Manassas, USA), samples were transferred to a microcentrifuge and spun down at 4 °C for 15 min at 13,000 rpm (Microcentrifuge 5415 R; Eppendorf, Stevenage, UK). The protein concentration was determined using the ND-1000 spectrophotometer (Nanodrop®, Wilmington, USA) and the appropriate amount of protein was transferred into an eppendorf. An equal volume of 2x sample buffer (Sigma-Aldrich) was added and the mixture was incubated at 95 °C for 10 min in a dry heating block (AccuBlock™ Digital Dry Bath; Labnet, Woodbridge, USA).

Table 2.2 Lysis stock buffer components

Stock reagents	Amount	Final concentration
1 M Tris-HCl pH 7.6 [a]	1.25 ml	50 mM Tris-HCl pH 7.6
NaCl [b]	200 mg	137 nM NaCl
Glycerol [b]	2.5 ml	10 % glycerol
Igepal [b]	0.025 ml	0.1 % Igepal
10 % SDS [c]	0.250 ml	0.1 % SDS
2 % NaF [a]	2.626 ml	50 mM NaF
dH_2O	25 ml	

[a] Sigma Aldrich
[b] VWR, Haasrode, Belgium
[c] AppliChem, Darmstadt, Germany

Samples were loaded onto a 4 – 15 % precast gel (Mini-PROTEAN® TGX; Bio-Rad, Hercules, USA), alongside a protein ladder (Precision Plus Protein Standard, Bio-Rad) and the gel was run at 250 V. Following electrophoresis, the proteins were transferred onto a nitrocellulose membrane (Trans-Blot®; Bio-Rad) for 1 h at 95 V in 1x Tris/Glycine buffer (Bio-Rad) with 10 % methanol (Sigma-Aldrich).

2.2.2. Immunoblotting and chemiluminescent detection

The membrane was blocked with blocking buffer [5 % milk powder in 1x TBST (0.1 % Tween 20 (Sigma-Aldrich) in 1x TBS)] for 1.5 h at RT and then incubated with the primary antibody at 4 °C overnight (Table 2.3). The membrane was then washed with 1x TBST and incubated with a mouse or rabbit horseradish peroxidase (HRP) - conjugated secondary antibody (1:5,000 dilution; anti-mouse/rabbit IgG; Invitrogen by Life Technologies) for 1 h at RT. The membrane was then washed with TBST and covered with ECL solution (Pierce® ECL Western Blot Substrate; Thermo-Scientific, Rockford, USA) for 2 min. In a dark room, blue-light sensitive film (SuperRX Fuji Medical X-Ray film; Fujifilm,

Bedford, UK) was placed in a film cassette with the membrane for varying exposure times and developed using an automated X-ray film processor (Compact X4; Xograph Imaging Systems, Tetbury, UK).

Table 2.3 Primary antibodies used in experimental studies

All reagents were purchased from Cell Signalling (Danvers, USA), unless otherwise stated.

Antibody	Species	Protein Size (kDa)	Dilution
β-Actin [a]	Mouse monoclonal	42	1:5,000
AKT	Rabbit polyclonal	60	1:2,000
Phospho-AKT (T308)	Rabbit monoclonal	60	1:1,000
γH2AX (S139) [b]	Mouse monoclonal	15	1:500
PARP	Rabbit polyclonal	116	1:500
PDK1	Rabbit monoclonal	58-68	1:1,000
Phospho-PDK1	Rabbit monoclonal	58-68	1:1,000
Phospho-S6 (S240/244)	Rabbit monoclonal	32	1:1,000
p53 [c]	Mouse monoclonal	53	1:2,000

[a] Sigma-Aldrich
[b] Millipore, Watford, UK
[c] Santa Cruz Biotechnologies, Heidelberg, Germany

2.3. Cell Proliferation Assay

Exponentially growing cells were seeded in 96-well plates (Corning Incorporated) at a density of 1,000 cells/well (triplicate wells of each sample). Following overnight incubation the drugs were added at the required concentrations and the plates were returned to the incubator. After five days, 20 µl of 1x resazurin (5 µg/ml; Sigma-Aldrich) was added to each well and plates were returned to the incubator for 4 h. Fluorescence intensity of resazurin was measured using a plate reader (POLARstar omega; BMG LABTECH, Aylesbury, UK; Ex 540 nm, Em 590 nm). The average fluorescence intensity was normalised to 100 % proliferation and plotted versus the drug concentration. The IC_{50} values were calculated using CalcuSyn v.2.0 (Biosoft, Cambridge, UK).

2.4. Clonogenic Survival Assay

Exponentially growing cells were plated in triplicate wells (3×10^2 – 3×10^3 cells/well) in 6-well plates, and allowed to attach overnight in standard culture conditions. The following day the drug was added to the wells 1 h before γ-irradiation using the Gamma Services GSR D1 irradiator with a Cs-137 source (dose rate of 1.69 Gy/min). The appropriate control was set up for each treatment and control cells were mock irradiated. Twenty-four hours after radiation exposure, the cells were washed with 1x PBS and fresh medium was added. Plates were incubated for 6 to 13 days to allow colonies to form. Cells were fixed and stained with 0.5 % crystal violet (Merck, Darmstadt, Germany) in 70 % methanol. Following air-drying, the number of colonies was counted manually.

The plating efficiency (PE) was calculated using the equation:

$$PE\ (\%) = \frac{number\ of\ colonies\ counted}{number\ of\ cells\ seeded}\ x\ 100$$

Following treatment, the surviving fraction (SF) was determined using the equation:

$$SF = \frac{PE\ treated\ cells}{PE\ control\ cells}$$

The radiation dose-response curves were generated by fitting the data to the linear quadratic model using the equation:

$$S(D) = e^{-\alpha D - \beta D^2}$$

in which S is function of cells surviving a dose D, and α and β are constants, representing the linear and quadratic components of cell killing.

The sensitisation enhancement ratio at 50 % (SER_{50}) cell survival was determined using the equation:

$$SER_{50} = \frac{D_{50}\ (untreated)}{D_{50}\ (drug\ treated)}$$

in which D_{50} is the radiation dose required to reduce cell survival to 50 %. The clonogenic survival curves and the SER_{50} were generated using OriginPro 8.5.1 (OriginLab®, Northampton, USA).

2.5. Immunofluorescence of γH2AX Foci

Cells were seeded at 2 x 10^4 cells/well in 96-well plates. The following day, cells were treated with dimethyl sulfoxide (DMSO; Fisher Scientific, Waltham, USA) or olaparib 1 h before exposure to γ-irradiation. Two and twenty-four hours after radiation treatment, cells were washed with 1x PBS and fixed with 100 µl of 3 % paraformaldehyde in 1x PBS (PFA; VWR) for 10 min at RT. Cells were then washed and blocked with 100 µl of 0.1 % Triton X (VWR), 1 % BSA (Sigma-Aldrich), and 1 % goat serum (Millipore) in 1x PBS for 1 h at RT. The cells were incubated overnight at 4 °C with mouse anti-human γH2AX antibody (1:1,500 dilution; Millipore) in 50 µl of 1 % BSA and 1 % goat serum in 1x PBS. Cells were then washed and incubated for 1 h at RT with Alexa Fluor® 488 goat anti-mouse (1:1,200 dilution; Invitrogen) and Hoechst (5 µg/ml; Sigma-Aldrich) in 50 µl of 1 % BSA in 1x PBS at RT. Cells were then washed and stored in 200 µl of 1x PBS at 4 °C in the dark until analysis. The 96-well plates were visualised on an automated fluorescent microscope (In Cell Analyser 1000; GE Healthcare, Chalfont St Giles, UK). Average foci count was acquired using IN Cell analysis software (triplicate wells, 10 random fields per well).

2.6. In Vivo Studies

Experimental protocols were approved by the Ethics Committee of Oxford University and the Home Office (project license 30/2834).

2.6.1. Preparation of cells for implantation

Cells were seeded in 75 cm^2 tissue culture flasks. Cells in exponential phase were washed once with ice-cold 1x PBS, detached, and counted as previously described in Section 2.1. Cells were then centrifuged for 3 min at 1200 rpm, and a cell suspension was prepared at a concentration of 1×10^8 Calu-3 cells/ml or 2×10^7 Calu-6 cells/ml in a 1:1 mix of serum-free Advanced DMEM medium and matrigel (BD Matrigel™ Matrix; BD Biosciences, Bedford, USA) before implantation.

2.6.2. Tumour xenograft initiation and measurements

To initiate tumour xenografts, 6 - 8 week old female BALB/c nude mice (Harlan Laboratories, Blackthorn, UK) were anaesthetised with 2.5 % isoflurane (IsoFlo®; Abbott Laboratories, Maidenhead, UK). Once anaesthetised, mice were ear clipped for identification purposes, followed by a dorsal subcutaneous injection of 0.1 ml cell suspension, approximately 1 cm from the base of the tail. Mice were kept in individual ventilated cages and subjected to a 12 h light and dark cycle. The general condition of the mice was monitored daily, and the tumours were measured with callipers three times per week. The tumour volume was calculated using the equation:

$$Volume\ (mm^3) = length\ x\ width\ x\ height\ x\ \frac{1}{2}$$

Once the tumour size reached 100 mm^3, the mice were randomized into treatment groups. The tumour size was measured three times per week until the tumour reached 500 mm^3 (relative tumour volume x 5; RTV5), or until day 42 after initiation of treatment, whichever occurred first. Tumour growth time (TGT3) was calculated as the time required for tumours to reach a 3-fold increase in relative tumour volume. Tumour growth delay (TGD) and percentage ratio (T/C %) were calculated using the equations:

$$TGD = TGT_{treated} - TGT_{control}$$

$$T/C\ \% = \frac{RTV\ treated}{RTV\ control}$$

2.6.3. Irradiation of tumours and treatment schedules

For radiation treatment, a tumour bearing mouse was injected IP with 0.1 ml of an anaesthetic cocktail [10 % Domitor® (Orion Pharma, Espoo, Finland) and 10 % Ketaset® (Pfizer, Tadworth, UK) in saline], and positioned in a lead tube to allow exposure of the tumour whilst shielding of the normal tissues. Mice were injected with olaparib (50 mg/kg IP) or vehicle [10 % DMSO in PBS/10 % 2-hydroxyl-propyl-β-cyclodextrin (Sigma-Aldrich)] 30 min before 10 Gy x-irradiation (320 kV Gulmay cabinet; Gulmay Medical Ltd., Surrey, UK). A dose rate of 1.81 Gy/min was administered (300 kV and 10 mA). The details of the different treatments are shown in Table 2.4 and Table 2.5.

Table 2.4 Treatment schedule radiation studies

Olaparib was injected IP (50 mg/kg) 30 min before irradiation and the vehicle was 10 % DMSO in PBS/10 % 2-hydroxyl-propyl-β-cyclodextrin.

	Day 1	**Day 2**	**Day 3**
Vehicle	Vehicle	Vehicle	Vehicle
Olaparib	Olaparib	Olaparib	Olaparib
10 Gy	10 Gy	/	/
Olaparib + 10 Gy	Olaparib + 10 Gy	Olaparib	Olaparib

Table 2.5 Treatment schedule imaging study

Olaparib was injected IP (50 mg/kg) and the vehicle was 10 % DMSO in PBS/10 % 2-hydroxyl-propyl-β-cyclodextrin.

	0 h	**2 h**	**24 h**	**26 h**
Vehicle	MRI	Vehicle	Vehicle	MRI
Olaparib	MRI	Olaparib	Olaparib	MRI

2.6.4. Tumour processing and histology

At the experimental endpoint, mice were sacrificed using cervical dislocation and the tumours were harvested: one half was snap frozen while the other half was fixed for 24 h in 3 % PFA in 1x PBS. Fixed samples were processed (Excelsior ES Tissue Processor; Thermo Scientific, Runcorn, UK) and embedded in paraffin wax. A TMA block was prepared as previously described (Kampf, Olsson et al. 2012). Briefly, two relevant tissue cores (length of 4 mm and diameter of 1 mm) of each PFA fixed paraffin embedded (PFPE) tumour were transferred to one recipient paraffin block. Serial sections of 4 µm thickness were obtained, and placed on a Superfrost glass slide (VWR). The slides were dried overnight at 37 °C and stored in a dark place at RT until processing for immunohistochemistry.

2.6.5. Immunohistochemistry

The slides were deparaffinised and rehydrated after incubation for 10 min at 50 °C (Table 2.6). Subsequently, heat-induced antigen retrieval was carried out by incubating slides in citrate buffer (1 g citric acid monohydrate in 500 ml dH_2O; pH 6.0) for 2 min at 110 °C and allowed to cool down for 20 min at RT. Slides were then stained for five different antibodies using the Dako envision G/2 Doublestain System kit (Dako Ltd., Ely, UK; Table 2.7; Table 2.8), counterstained with hematoxylin for 30 sec and mounted with aqueous mounting medium (Aquatex®, Millipore) and covered with a coverslip. Slides were scanned the following day (ScanScope CS; Aperio Technologies, Vista, USA) and analysed using ImageScope analysis software (Aperio Technolgies).

Table 2.6 Deparaffinisation and rehydration process

Step	Reagent	Time (min)
1	Citroclear	5
2	Citroclear	5
3	100 % ethanol	3
4	100 % ethanol	3
5	70 % ethanol	3
6	50 % ethanol	3
7	dH_2O	5

Table 2.7 Primary antibodies used for immunohistochemistry

Antibody	Dilution	Manufacturer
γH2AX	1;1,000	Millipore
CAIX	1:100	NDCLS [a]
CC3	1:600	Cell Signalling
CD31	1:50	Abcam [b]
Ki67	1:1,000	Millipore

[a] Nuffield Division of Clinical Laboratory Sciences, University of Oxford, UK
[b] Cambridge, UK

Table 2.8 Dako Envison G/2 Doublestain process

Slides were washed between each step in 1x PBS with 0.1 % Tween-20 and incubations were performed at RT unless otherwise stated.

Step	Reagent	Time (min)
1	Dual Endogenous Enzyme Block	20
2	Primary Antibody	60
3	Polymer/HRP	20
4	DAB+ Working Solution	2
5	Doublestain Block	15
6	Primary Antibody (4 °C)	overnight
7	Rabbit/Mouse (LINK)	20
8	Polymer/AP	20
9	Permanent Red Working Solution	10

2.6.6. Dynamic contrast enhanced-magnetic resonance imaging (DCE-MRI)

MRI was performed on tumour bearing mice (100 mm^3) before and after treatment (vehicle or olaparib 50 mg/kg IP) at 4.7 Tesla (Agilent Technologies, Stockpost, UK) using a 25-mm quadrature birdcage coil (RAPID Biomedical, Rimpar, Germany; Figure 2.1). Respiration-gated 3D gradient echo imaging (TE = 0.55 ms, TR = 1.1 ms) covering a field of view of 54 x 27 x 27 mm at an isotropic resolution of 0.42 mm was used for the DCE. One hundred repetitions of the scan were acquired with gadodiamide contrast agent (Gd; Omniscan™, GE Healthcare). During acquisition of image frame 11/100, Gd (30 µl) was infused via a tail vein cannula over approximately 5 sec. The DCE-MRI signal was converted to Gd concentration using the method described by Schabel and Parker (2008). The tumour region was manually segmented from an average image of the DCE-MRI time course using ITK-SNAP (Yushkevich, Piven et al. 2006). The initial area under the Gd uptake curve was calculated for the first 90 sec on a voxel by voxel basis, and the median for the tumour and muscle regions obtained.

2.7. Compound Formulation

Olaparib and BX912 were purchased from Selleck (Munich, Germany). GSK2334470 was purchased from Tocris Bioscience (Bristol, UK). For *in vitro* studies, 10 mM stock solutions of the drugs were prepared in 100 % DMSO and kept at -20 °C until use. For *in vivo* studies, olaparib was administered intra-peritoneal (IP) at a dose of 50 mg/kg in vehicle (10 % 2-hydroxyl-propyl-β-cyclodextrin in 1x PBS).

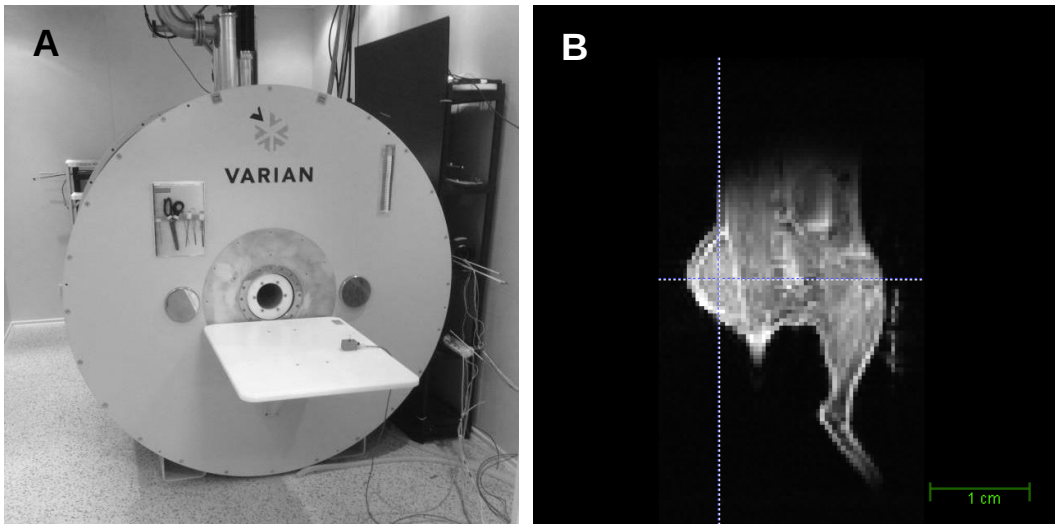

Figure 2.1 Magnetic resonance imaging

(A) 4.7 T MRI system, (B) Sagittal DCE-MRI image with the xenograft indicated by crosshairs.

2.8. Statistical Analysis

IBM SPSS Statistics 20 (IBM, Portsmouth, UK) was used for statistical comparison between two groups using Student's *t*-test, and between more than two groups by analysis of variance (ANOVA). MedCalc 12.7.0 (MedCalc Software, Ostend, Belgium) was used to generate *in vivo* Kaplan-Meier survival curves. All data was expressed as mean values ± standard error of the mean (SEM). P values <0.05 were considered significant.

CHAPTER 3

Results

3. Results

3.1. Effects of PDK1 inhibition *in vitro*

Inhibition of the PI3K/AKT/mTOR pathway has shown promise in preclinical studies combined with radiation therapy. Therefore, we sought to determine the potential of PDK1 inhibitors as radiosensitising agents in the treatment of NSCLC. Since reciprocal regulation between the PI3K-AKT and p53 signalling pathways has been suggested (Fei and El-Deiry 2003), we first investigated the p53 protein expression levels by western blotting in the cells lines to be used in these studies (Figure 3.1). Protein expression levels were consistent with reported *TP53* mutation status for each of the cell lines tested (cell lines H1975, A549, and H1299 are *TP53* mutant, wild-type and null, respectively) (Bamford, Dawson et al. 2004).

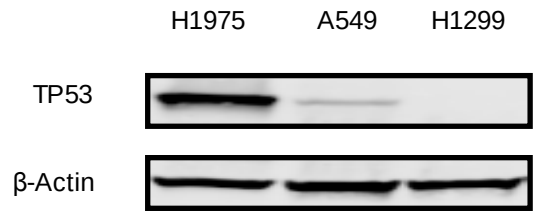

Figure 3.1 *TP53* status of NSCLC cell lines

NSCLC cell lines (H1975, A549 and, H1299) were lysed and analysed by western blotting to confirm their *TP53* status (mutant, wild-type, and null, respectively).

Subsequently, we assessed the impact of two PDK1 inhibitors (GSK2334470 and BX912) on cell viability using a resazurin-based cell proliferation assay. The three cell lines were exposed to increasing concentrations of the PDK1 inhibitors (0-9 μM) for 5 days before assessment of cell viability.

Each inhibitor showed a dose-dependent decrease in cell proliferation (Figure 3.2). Both drugs had a similar cytotoxicity in the lines H1975 and A549, whereas in H1299, BX912 was more cytotoxic in the 2-7 μM range compared with GSK2334470. The IC_{50} values (the dose at which 50 % of cell proliferation is inhibited) was determined for both drugs in each cell line (Table 3.1).

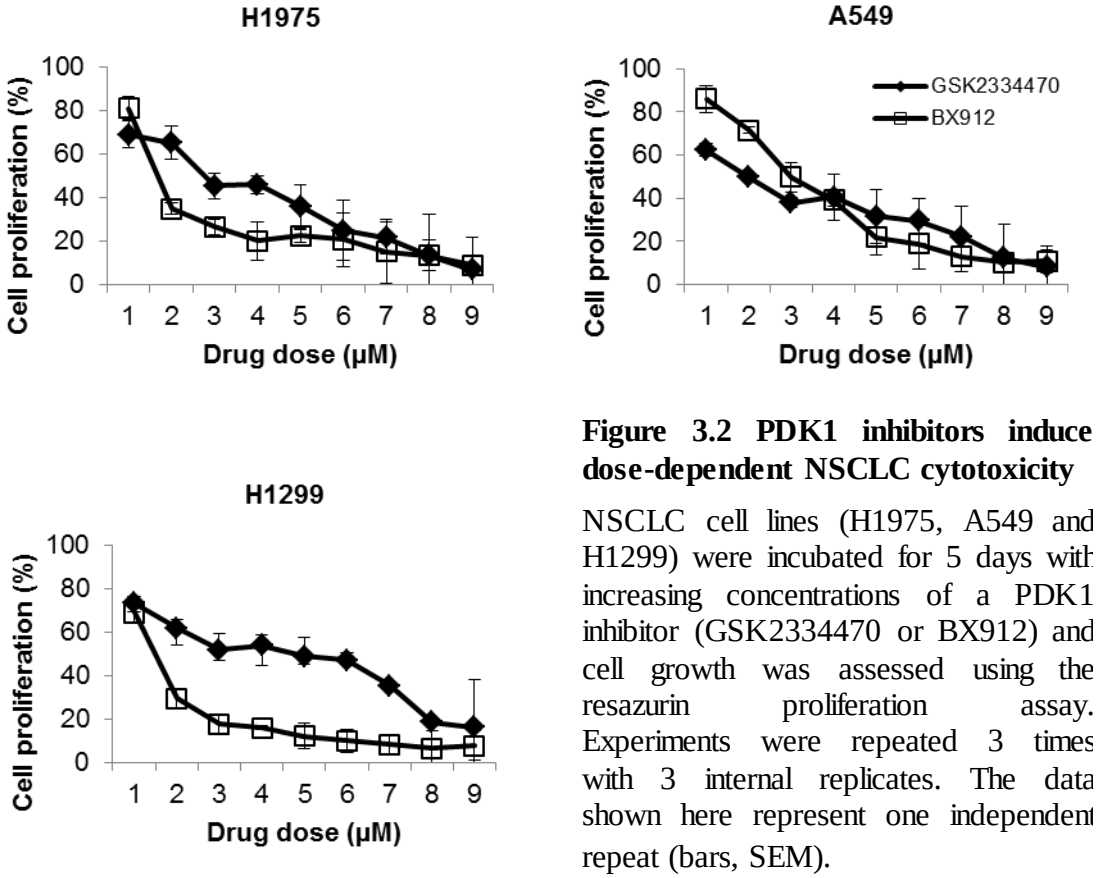

Figure 3.2 PDK1 inhibitors induce dose-dependent NSCLC cytotoxicity

NSCLC cell lines (H1975, A549 and H1299) were incubated for 5 days with increasing concentrations of a PDK1 inhibitor (GSK2334470 or BX912) and cell growth was assessed using the resazurin proliferation assay. Experiments were repeated 3 times with 3 internal replicates. The data shown here represent one independent repeat (bars, SEM).

Table 3.1 IC_{50} values of the PDK1 inhibitors GSK2334470 and BX912

	GSK2334470 (μM)	BX912 (μM)
H1975	2.5	1.9
A549	2.0	2.8
H1299	3.3	1.3

Radiation exposure of human glioblastoma cell lines has previously been shown to upregulate pAKT levels, thereby increasing anti-apoptotic signalling (Li, Kim et al. 2009) and therefore providing a rationale for combining inhibition of AKT signalling with radiation. We showed that 2 h after 10 Gy radiation exposure, pAKT levels of A549 cells increased compared with the levels of mock irradiated A549 cells (Figure 3.3). The pAKT levels of H1299 cells were not altered after radiation exposure or olaparib treatment (data not shown).

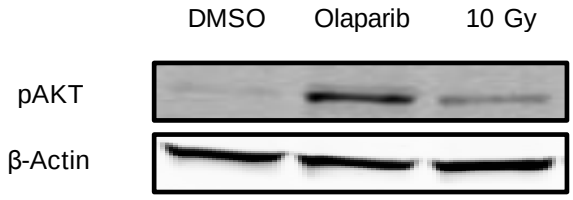

Figure 3.3 Both radiation and olaparib exposure induce pAKT upregulation
A549 cells were exposed to 0.05 % DMSO, 5 µM olaparib, or 10 Gy, and cells were lysed 2 h after treatment. Lysates were analysed for pAKT levels by western blotting.

Inhibition of downstream signalling by the PDK1 inhibitor GSK2334470 was assessed after 24 h continuous exposure to the drug. For the cell lines A549 and H1299 we demonstrated that a 0.2 µM concentration of GSK2334470 partially inhibited phosphorylation of S6 (a downstream target of PDK1). Substantial inhibition of S6 phosphorylation by GSK2334470 was observed at doses ≥1 µM (Figure 3.4). Based on these results and the results of the cell proliferation assays, we selected a PDK1 inhibitor dose of 1 µM for *in vitro* radiosensitisation experiments.

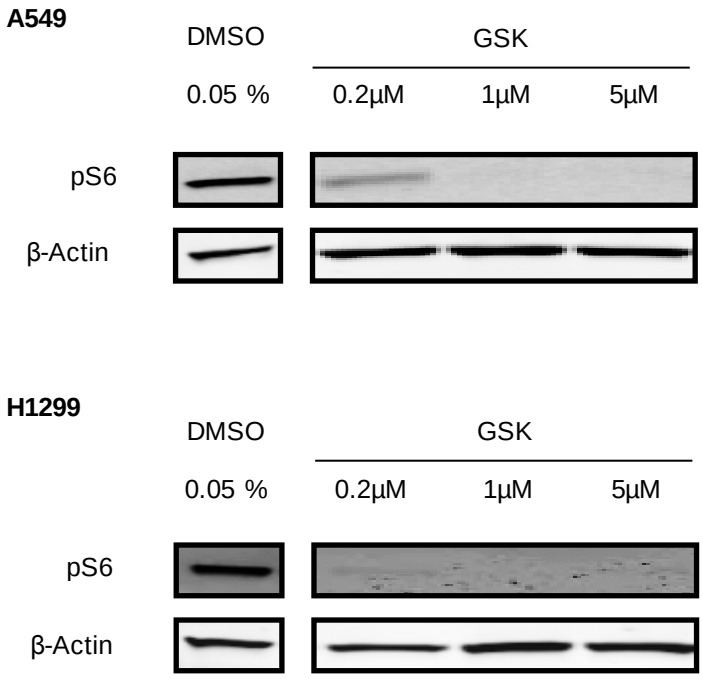

Figure 3.4 Inhibition of downstream signalling by GSK2334470
Cells were exposed to GSK2334470 and were lysed after 24 h. Lysates were analysed for pS6 levels by western blotting.

To assess the impact of PDK1 inhibition on the radiation response of NSCLC cell lines, we studied the three NSCLC cell lines in clonogenic survival assays, either alone or in combination with a PDK1 inhibitor (GSK2334470 or BX912). Cells were incubated with 1 µM of the PDK1 inhibitor or 0.05 % DMSO 1 h before radiation exposure. The drug-containing medium was replaced with fresh medium 24 h after radiation and the plates were returned to the incubator until sufficiently large colonies were formed (>50 cells per colony). A dose-dependent decrease in clonogenic survival was observed for each cell line. We showed that treatment with 1 µM of a PDK1 inhibitor 1 h before radiation exposure does not alter the intrinsic radiosensitivity of the investigated NSCLC cell lines (Figure 3.5).

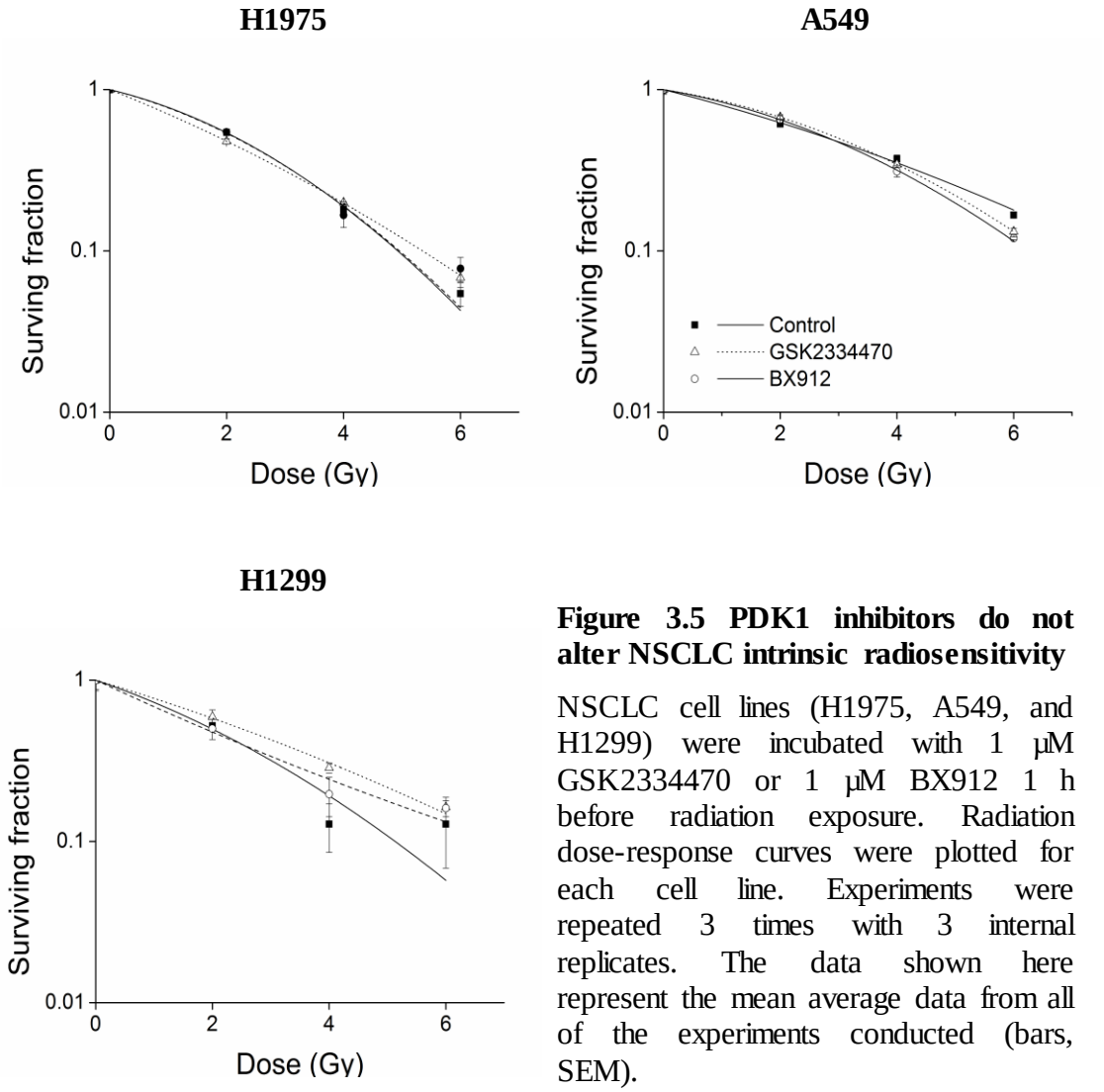

Figure 3.5 PDK1 inhibitors do not alter NSCLC intrinsic radiosensitivity

NSCLC cell lines (H1975, A549, and H1299) were incubated with 1 μM GSK2334470 or 1 μM BX912 1 h before radiation exposure. Radiation dose-response curves were plotted for each cell line. Experiments were repeated 3 times with 3 internal replicates. The data shown here represent the mean average data from all of the experiments conducted (bars, SEM).

3.2. Effects of olaparib *in vitro*

Recently, the radiosensitising potential of PARP inhibition has been recognised in NSCLC (Senra, Telfer et al. 2011). Based on these findings, we investigated the radiosensitising characteristics of the PARP inhibitor olaparib in NSCLC. First, we determined the impact of olaparib on cell viability using a resazurin-based cell proliferation assay. Three NSCLC cell lines were exposed to increasing concentrations of olaparib (0–10 μM) for five days before assessment of cell viability. Exposure to 5 μM olaparib for five days did not induce significant antiproliferative effects in any of the cell lines tested (Figure 3.6).

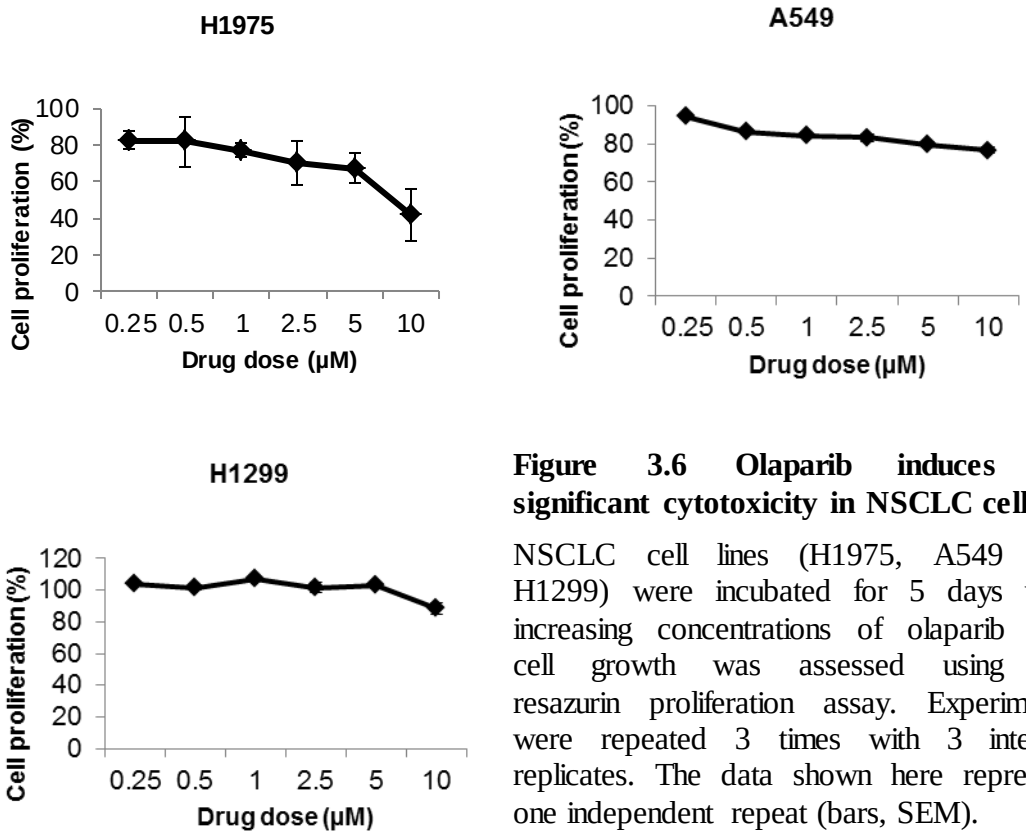

Figure 3.6 Olaparib induces no significant cytotoxicity in NSCLC cells

NSCLC cell lines (H1975, A549 and H1299) were incubated for 5 days with increasing concentrations of olaparib and cell growth was assessed using the resazurin proliferation assay. Experiments were repeated 3 times with 3 internal replicates. The data shown here represent one independent repeat (bars, SEM).

Subsequently, we studied a panel of five NSCLC cell lines and a normal tissue derived telomerase-immortalised normal bronchial epithelial cell line NBE1 (Stead, Berri et al. 2012) in clonogenic survival assays, either alone or in combination with 5 µM olaparib. A dose-dependent decrease of the surviving fraction was observed for each cell line. H1299 was the most radioresistant cell line, and the bronchial-epithelial cell line NBE1 was the most radiosensitive (Figure 3.7). The SER_{50} of 5 µM olaparib was calculated using the linear quadratic model (Table 3.2). While pre-treatment with 5 µM olaparib 1 h before radiation exposure clearly enhanced the radiosensitivity of each of the five investigated NSCLC cell lines (SER_{50} 1.6 to 2.2), the bronchial epithelial cell line NBE1 was less radiosensitised (SER_{50} 1.2).

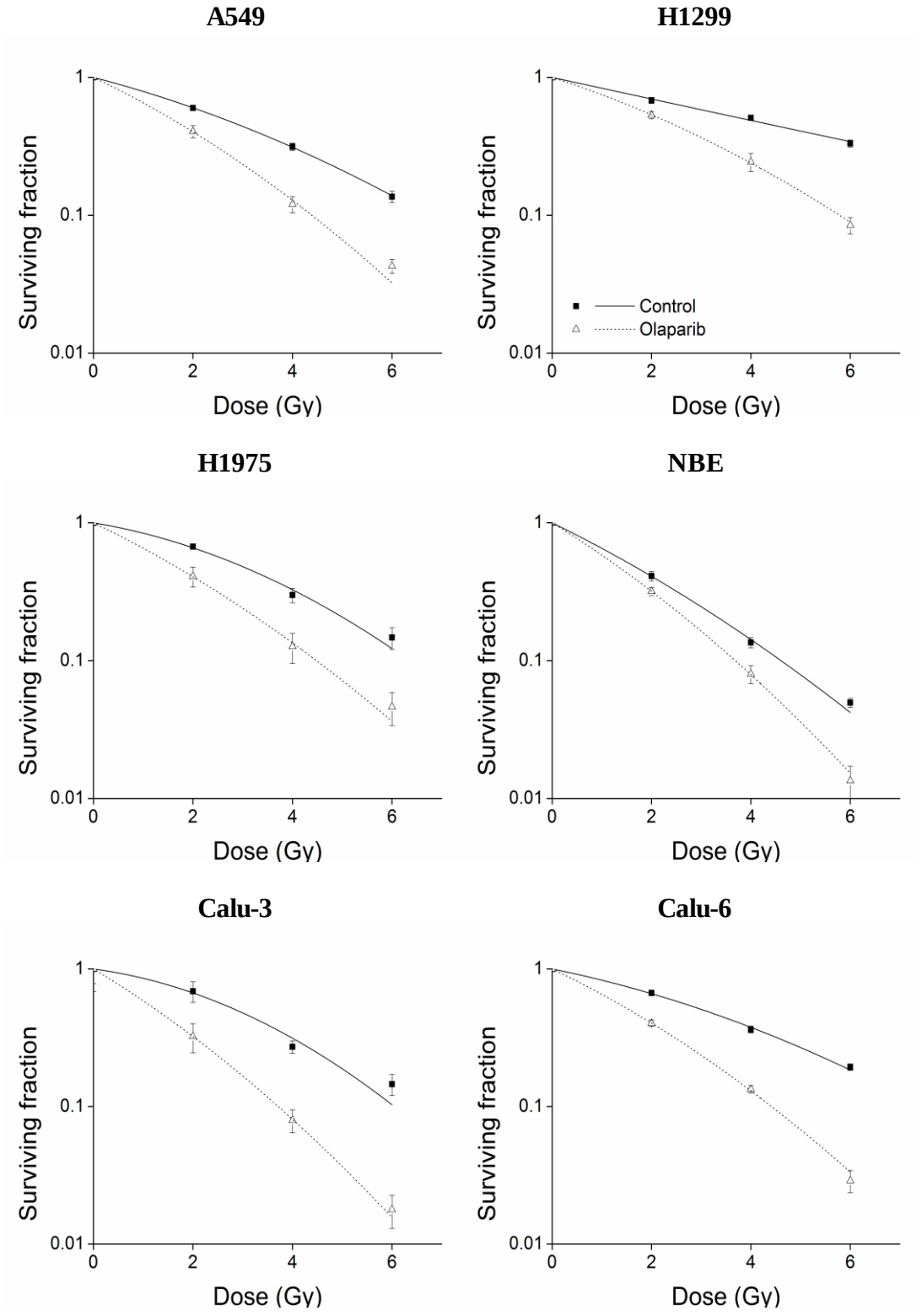

Figure 3.7 Olaparib potentiates the cytotoxicity of radiation treatment of five NSCLC cell lines

NSCLC cell lines were incubated with 5 µM olaparib or 0.05 % DMSO 1 h before radiation exposure. Radiation dose-response curves were plotted for each cell line. Experiments were repeated 3 times with 3 internal replicates. The data shown here represent the mean average from all of the experiments conducted (bars, SEM).

Table 3.2 Sensitisation enhancement ratio of 5 µM olaparib

Cell line	D_{50} untreated	D_{50} olaparib treated	SER_{50}
A549	2.61	1.57	1.6
H1299	3.86	2.19	1.7
H1975	2.89	1.58	1.8
NBE1	1.58	1.26	1.2
Calu-3	2.89	1.28	2.2
Calu-6	3.06	1.57	1.9

Olaparib is an effective PARP inhibitor which we confirmed by western blotting. Calu-6 and Calu-3 were irradiated with 0 or 10 Gy in the presence or absence of 5 µM olaparib. Cells were lysed 2 and 24 h after treatment. Twenty-four hours after 10 Gy radiation exposure, an increase in PARP ribosylation (seen as a high-molecular weight smear on the western-blot) was observed which was not present after combination treatment (Figure 3.8). For both cell lines we showed that 24 h after olaparib or combination treatment, PARP poly(ADP) ribosylation was inhibited. At the 2 h time-point, no effect of olaparib exposure was observed.

Cleaved PARP is an indicator of cells undergoing apoptosis (Oliver, de la Rubia et al. 1998), and its formation can be also analysed by western blotting. Calu-6 cells treated with olaparib or exposed to radiation, showed increased levels of cleaved PARP 24 h after treatment (Figure 3.8). The combination treatment increased levels of cleaved PARP even further. No changes in cleaved PARP levels were observed at the 2 h time-point. Calu-3 cells showed no induction of cleaved PARP.

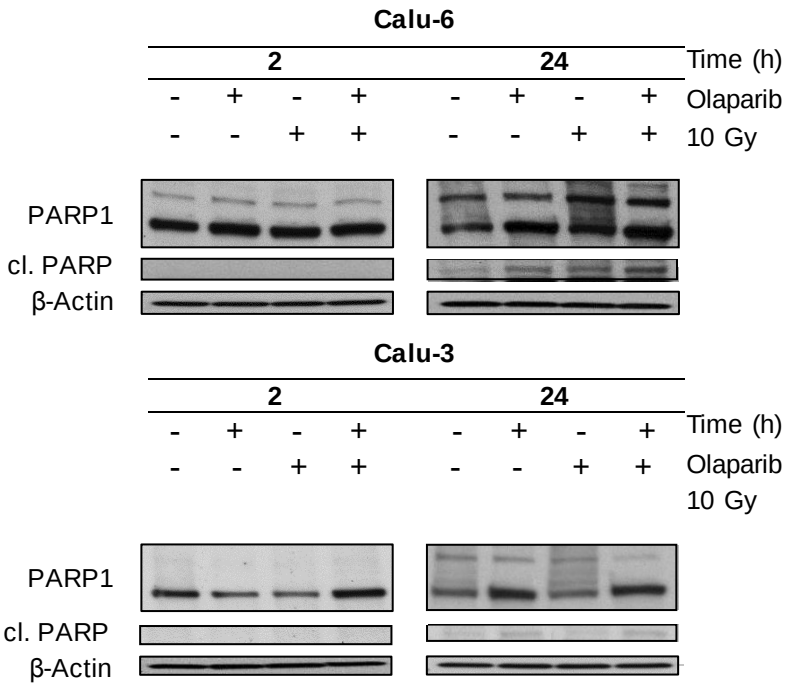

Figure 3.8 Olaparib prevents poly(ADP) ribosylation

Calu-6 and Calu-3 cells were exposed to radiation in the presence or absence of 5 μM olaparib and were lysed 2 and 24 h after treatment. Lysates were analysed for PARP1 and cleaved PARP by western blotting.

PARP inhibition compromises DNA repair by preventing access of DNA repair proteins to DNA SSBs. In the S phase of the cell cycle unrepaired SSBs can collide with the replication fork and eventually result in the formation of DSBs (Powell, Mikropoulos et al. 2010). A histone H2A family member (H2AX) becomes phosphorylated at serine-139 (γH2AX) by ATM, ATR or DNA-PK at sites of DNA DSBs. Therefore, the formation of γH2AX can be used as an indicator of DNA DSBs (Rogakou, Boon et al. 1999). We assessed the effect of olaparib on DNA repair in NSCLC by exposing Calu-6 and Calu-3 cells to radiation in the presence or absence of olaparib (0.05 % DMSO, 5 μM olaparib, 10 Gy radiation exposure, or 5 μM olaparib incubation 1 h before 10 Gy irradiation). Cells were lysed 2 and 24 h after treatment.

For both cell lines, an increase in γH2AX signal was observed 2 h after 10 Gy radiation exposure. Twenty-four hours after radiation exposure, the signal intensity had decreased, indicating that the majority of the DNA damage was repaired. When Calu-6 cells were incubated with olaparib 1 h before radiation exposure, a reduction in γH2AX signal intensity was observed at 24 h, compared with the signal intensity at 2 h. When Calu-3 cells were incubated with olaparib 1 h before radiation exposure, an increase in γH2AX signal intensity was observed at 24 h, compared with the signal intensity at 2 h (Figure 3.9). These results indicate that olaparib compromises the DNA repair after radiation exposure.

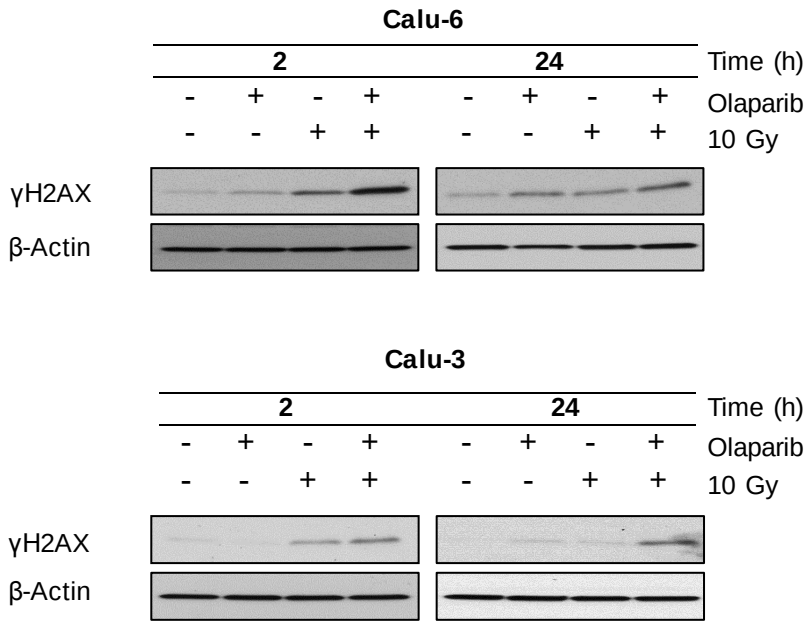

Figure 3.9 Olaparib compromises DNA repair after radiation exposure

Calu-6 and Calu-3 cells were exposed to radiation in the presence or absence of 5 μM olaparib and were lysed 2 and 24 h after treatment. Lysates were analysed for γH2AX by western blotting.

DNA repair was also quantified by measurement of γH2AX foci formation using immunofluorescence. Calu-6 and Calu-3 cells were incubated with 0.05 % DMSO or 5 μM olaparib 1 h before radiation exposure (0, 1, 2 or 10 Gy). Cells were fixed 2 and 24 h after treatment, and the average number of foci was acquired using an automated fluorescent microscope (IN Cell analyzer 1000, GE Healthcare). At the 2 h time-point, a dose-dependent increase in foci was observed in both the control and the olaparib treated groups (Figure 3.10). Twenty-four hours after 2 Gy radiation exposure, the number of foci had decreased in the control group (25 % in Calu-6 cells and 30 % in Calu-3 cells), compared with the 2 h time-point. In contrast, at the 24 h time-point, the number of foci in the combination treated (olaparib and 2 Gy) Calu-6 cells increased by an additional 50 %, and the amount of foci in the combination treated (olaparib and 2 Gy) Calu-3 cells decreased by 20 %, compared with the 2 h time-point ($P < 0.01$). Together, these findings suggest that DNA repair after radiation exposure is compromised by olaparib.

3.3. Effects of combined PDK1 and PARP inhibition *in vitro*

Exposure of the human hepatic cell line WRL-68 to the PARP inhibitor PJ-34 has been shown to upregulate pAKT levels, thereby increasing anti-apoptotic signalling (Tapodi, Debreceni et al. 2005). We showed that 2 h after incubation with 5 μM olaparib, pAKT levels of A549 cells were markedly increased compared with pAKT levels of DMSO-treated cells (Figure 3.3). Therefore, we hypothesised that addition of a PDK1 inhibitor (GSK2334470 or BX912) to the 1 h pre-treatment with olaparib could further enhance the radiosensitisation seen with olaparib, by decreasing the anti-apoptotic signalling induced by olaparib treatment.

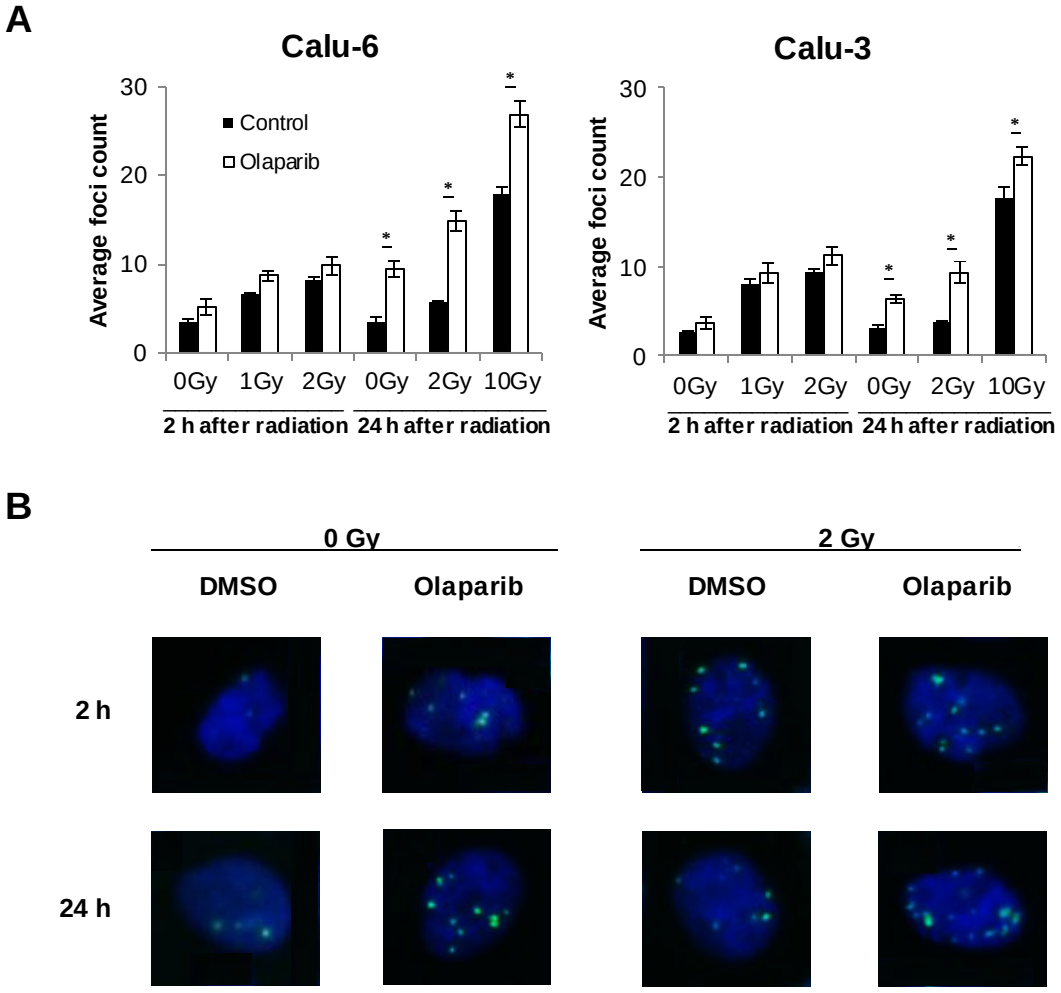

Figure 3.10 Olaparib decreases the DNA repair 24 h after radiation exposure

Calu-6 and Calu-3 cells were incubated with 0.05 % DMSO or 5 µM olaparib 1 h before radiation exposure (0, 1, 2 or 10 Gy). Cells were fixed 2 and 24 h after treatment. (A) average γH2AX foci count was acquired using the IN cell analyser 1000, (B) representative Calu-6 cellular images with green indicating γH2AX foci and blue indicating the nucleus (Hoechst) ($P < 0.01$). Experiments were repeated 3 times with 3 internal replicates. The data shown here represent one independent repeat (bars, SD).

Two NSCLC cell lines (H1975 and A549) were incubated for 1 h before radiation exposure with 5 µM olaparib, 1 µM GSK2334470 + 5 µM olaparib, or 1 µM BX912 + 5 µM olaparib. For the cell line H1975, we observed that a combined pre-treatment of a PDK1 inhibitor and olaparib did not alter the radiosensitisation induced by olaparib alone. For A549, we observed that the combined pretreatment reduced the radiosensitisation induced by olaparib treatment alone (Figure 3.11).

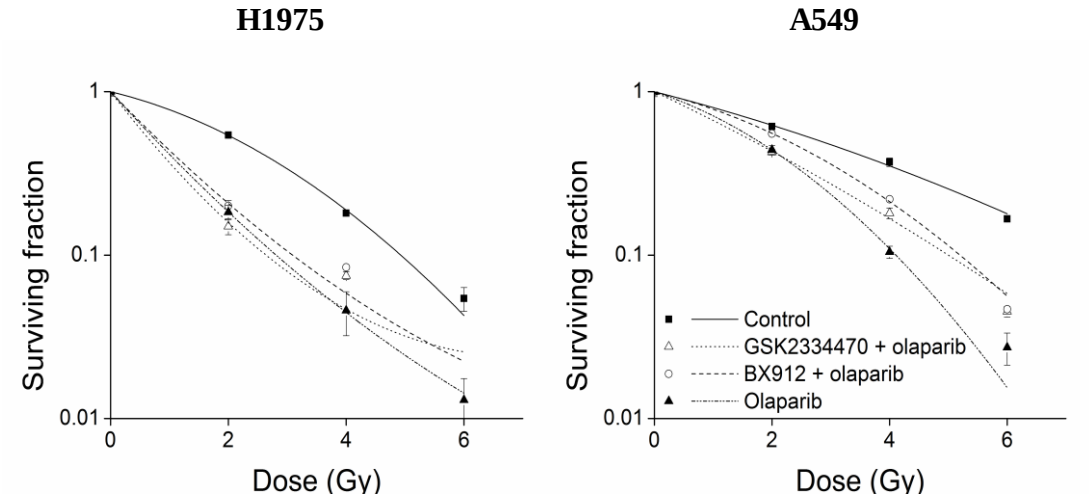

Figure 3.11 Combination treatment of PDK1 inhibitors and olaparib is not more beneficial than olaparib treatment alone

NSCLC cell lines (H1975 and A549) were incubated 1 h before radiation exposure with 5 μM olaparib, 1 μM GSK2334470 + 5 μM olaparib, or 1 μM BX912 + 5 μM olaparib. The drug-containing medium was replaced with fresh medium 24 h after radiation. Radiation dose-response curves were plotted for each cell line. Experiments were repeated 3 times with 3 internal replicates. The data shown here represent the mean average data from all of the experiments conducted (bars, SEM).

3.4. Effect of olaparib on tumour growth

We have shown that olaparib radiosensitises NSCLC cell lines *in vitro*, most likely due to inhibition of DNA repair resulting in increased levels of residual DNA DSBs (Figure 3.7 and 3.9). Next, we assessed the *in vivo* radiosensitising characteristics of olaparib in two subcutaneous xenograft models of NSCLC (Calu-6 and Calu-3). Tumour bearing mice were randomised into 4 experimental groups (n=6 for each treatment group): vehicle (daily for 3 consecutive days), olaparib (50 mg/kg IP daily for 3 consecutive days), 10 Gy radiation (on day 1), or olaparib combined with 10 Gy radiation (50 mg/kg olaparib IP daily for 3 consecutive days with irradiation 30 min after the first olaparib injection).

For *in vivo* studies we evaluated a 10 Gy dose of radiation in combination with 3 days treatment with olaparib. The irradiation dose was based on our *in vitro* data which suggested a 10 Gy treatment resulted in a significant increase in γH2AX (indicating unrepaired DNA DSBs) which was further increased by the combination with olaparib (Figure 3.9 and 3.10). Therefore, we designed our *in vivo* studies to include analysis of tumours from animals sacrificed 24 h after radiation to compare with our *in vitro* data.

Olaparib at 50 mg/kg has been widely used for anti-tumour studies in nude mice and results in intratumoral drug concentrations of >1μM and significant inhibition of PARP activity (Kortmann, McAlpine et al. 2011). *In vitro* studies have suggested that the majority of DNA DSBs are repaired within 24 h (Rothkamm, Kruger et al. 2003), although DNA DSBs are repaired more slowly under hypoxic conditions (Kumareswara, Ludkovski et al. 2012). We chose to treat for 3 days so we were able to assess the impact of olaparib on the repair of slowly repaired DNA DSBs, in particular those in hypoxic regions of the tumour.

3.4.1. Effect on tumour growth in Calu-6 xenografts

The individual tumour growth of the Calu-6 xenografts was plotted for each experimental group (Figure 3.12A). Where the vehicle and olaparib treated group showed marked variability in tumour growth, the radiation and combination treated group showed less variability.

Approximately two days after the initiation of treatment, both the radiation and combination group showed a reduction in growth, and by day five stable disease was achieved (Figure 3.12B). From day ten onwards, the radiation group re-initiated growth at a rate similar to the rate of the vehicle group, whereas the combination group showed a clear reduction in growth rate, compared with the radiation group. Tumour growth time to triple in volume (TGT3) was calculated for each experimental group and was 11 days, 13 days, 24 days, and 40 days (vehicle, olaparib, irradiation, and combination, respectively; Figure 3.13). Tumour growth delay was 2 days, 13 days and 29 days (olaparib, irradiation, and combination group, respectively), compared with the vehicle group. Olaparib treatment alone did not have a significant effect on the TGT of the Calu-6 xenograft model, compared with vehicle treatment. A significant growth delay (approximately 16 days) was observed for the combination group, when compared with radiation treatment alone ($P < 0.001$).

At day 17 (the day at which all animals in the vehicle group had been humanely killed), the average tumour volume of the olaparib group, the radiation group and the combination group was 80 %, 42 % and 27 % of the average tumour volume in the vehicle group, respectively.

Where olaparib treatment alone did not increase survival probability, a combined treatment of olaparib and radiation therapy increased the overall survival probability of the Calu-6 xenograft model compared with radiation alone ($P = 0.004$; Figure 3.14). No weight changes were noted after olaparib treatment alone or in combination with radiotherapy

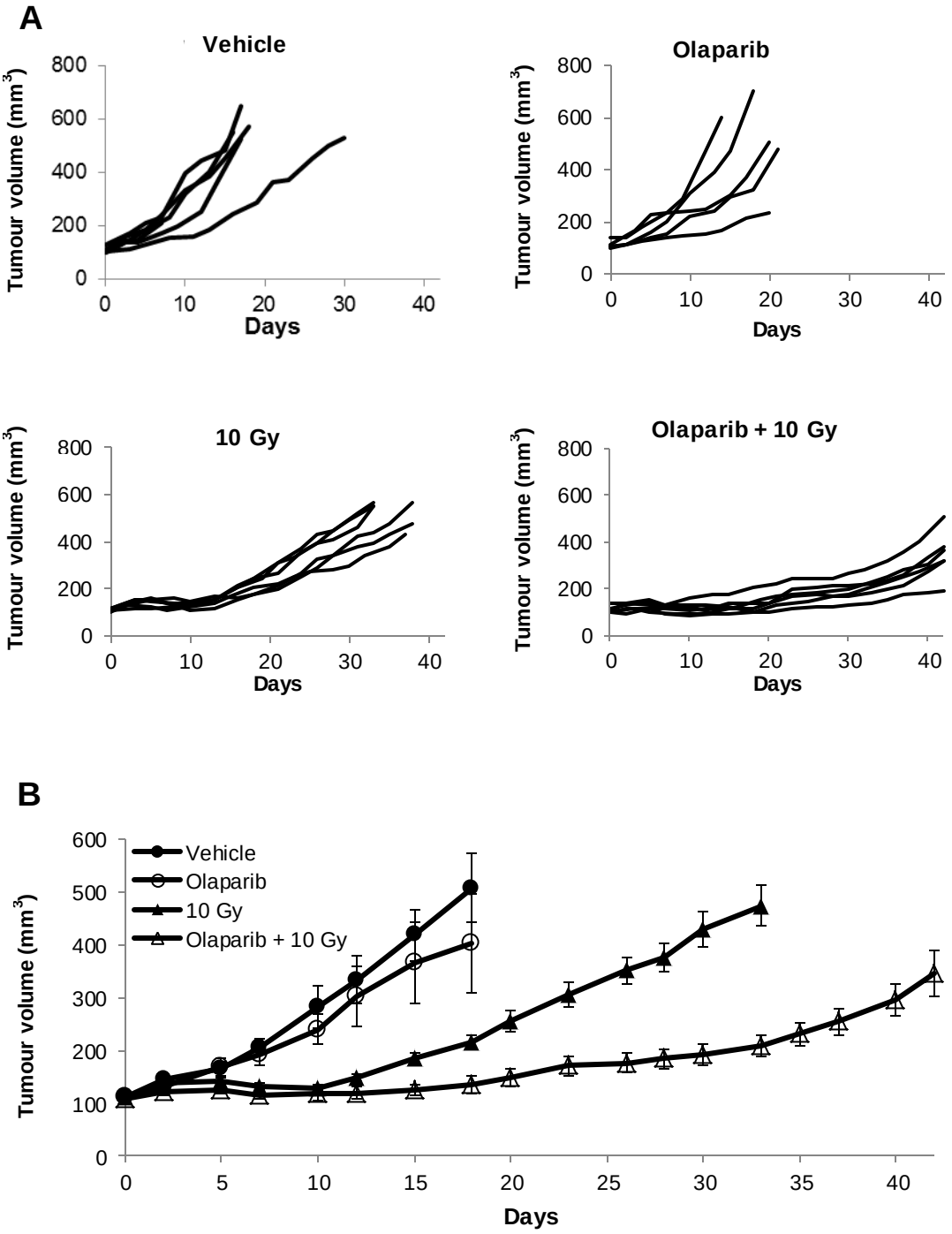

Figure 3.12 Combination treatment of radiation and olaparib induces a significant growth delay in Calu-6 subcutaneous xenografts

Mice were randomised into 4 groups with 5 animals/group: vehicle, olaparib (50 mg/kg IP), 10 Gy radiotherapy, or olaparib combined with 10 Gy radiotherapy. (A) individual tumour growth per group, (B) average tumour growth curves for all groups (bars, SEM).

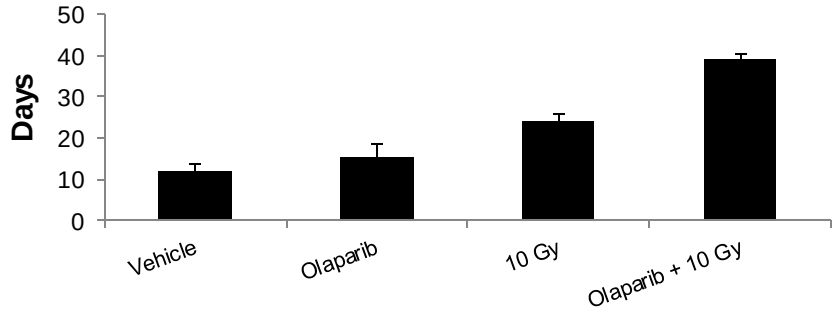

Figure 3.13 Combined treatment of olaparib and irradiation reduces the growth rate of Calu-6 subcutaneous xenografts

Average number of days that tumours needed to increase their initial volume by factor 3, was plotted for each experimental group (bars, SEM).

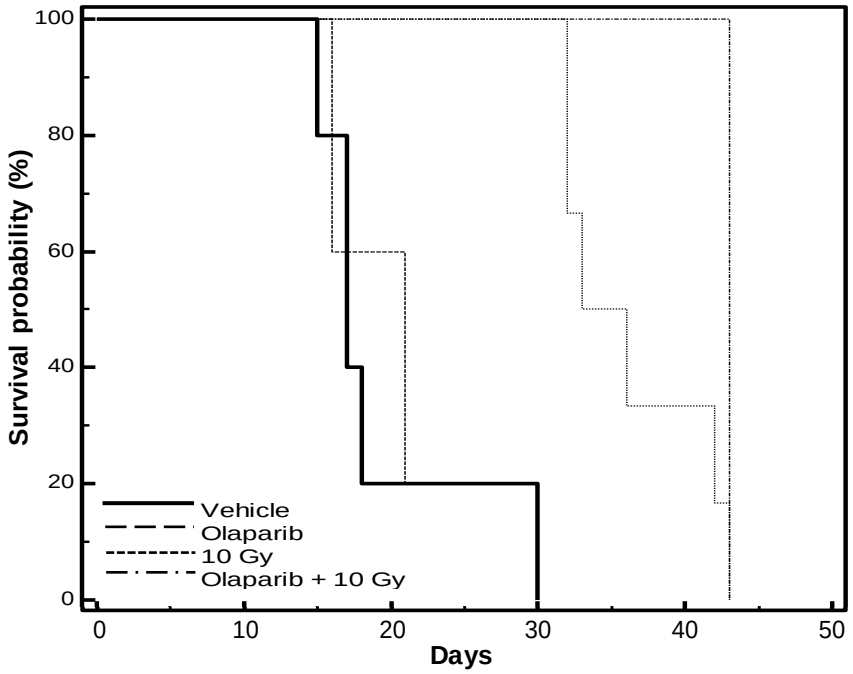

Figure 3.14 Survival probability of Calu-6 xenografts increases after combined treatment of olaparib and radiation

Kaplan-Meier plot of survival probability (TGT3) for Calu-6 bearing nude mice.

3.4.2. Effect on tumour growth in Calu-3 xenografts

A second NSCLC xenograft model (Calu-3) was established to confirm the radiosensitising characteristics of olaparib *in vivo* (Figure 3.15). Calu-3 xenografts grew considerably slower ($TGT_{vehicle}$ 11 days and 30 days for Calu-6 and Calu-3, respectively), and radiation therapy alone was more beneficial as monotherapy compared with the Calu-6 xenografts (TGT_{RTX} 24 days and >42 days for Calu-6 and Calu-3, respectively). Olaparib treatment alone did not have a significant effect on the growth of the Calu-3 tumour model, compared with vehicle treatment. The growth rate of the combination group did not differ from the growth rate of the radiotherapy alone group.

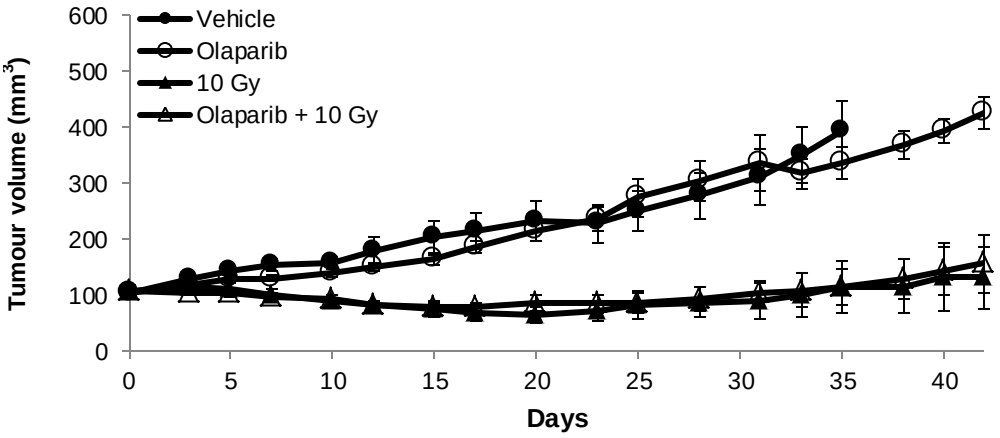

Figure 3.15 Combined treatment of olaparib and radiation induces no growth delay in Calu-3 subcutaneous xenografts

Mice were randomised into 4 groups with 5 animals/group: vehicle, olaparib (50 mg/kg IP), 10 Gy radiotherapy, or olaparib combined with 10 Gy radiotherapy. The average tumour growth volume for each group is plotted (bars, SEM).

3.5. Effect of olaparib on proliferation, apoptosis and DNA repair *in vivo*

To determine whether the tumour growth delay observed in Calu-6 xenografts treated with the combination of radiation and olaparib resulted from decreased proliferation, increased apoptosis and/or decreased DNA repair, histology sections were obtained from Calu-6 and Calu-3 xenografts 24 and 72 h after initiation of treatment (n=3 per time-point for each treatment group). The sections were immunostained for Ki67, γH2AX and Cleaved Caspase 3 (CC3).

3.5.1. Proliferation, apoptosis and DNA repair in Calu-6 xenografts

The Ki67 proliferative index varied between tumour samples (61 % - 72 %), but there was no difference between treatment groups. At the 24 h time-point, CC3 staining was similar in the radiation treated tumours and combination treated tumours, and was 1.6 times higher compared with the untreated tumours (Fig 3.16A and B). At the 72 h time-point, the radiation treated and combination treated tumours had 2 and 3 times more apoptotic cells compared with the untreated tumours, respectively ($P = 0.036$ for combination versus radiation treatment alone). As shown in Figure 3.16C and D, at the 24 h time-point, the number of γH2AX foci per cell was highest in combination treated tumours, 1.8 times more compared with radiation treated tumours, and 12 times more compared with untreated tumours. Although in both the radiation and combination treated tumours the number of foci per cell had decreased at the 72 h time-point, the combination treated tumours showed significantly higher amounts of γH2AX foci per cell ($P < 0.01$ for combination versus radiation alone), suggesting olaparib treatment inhibits DNA repair in this model.

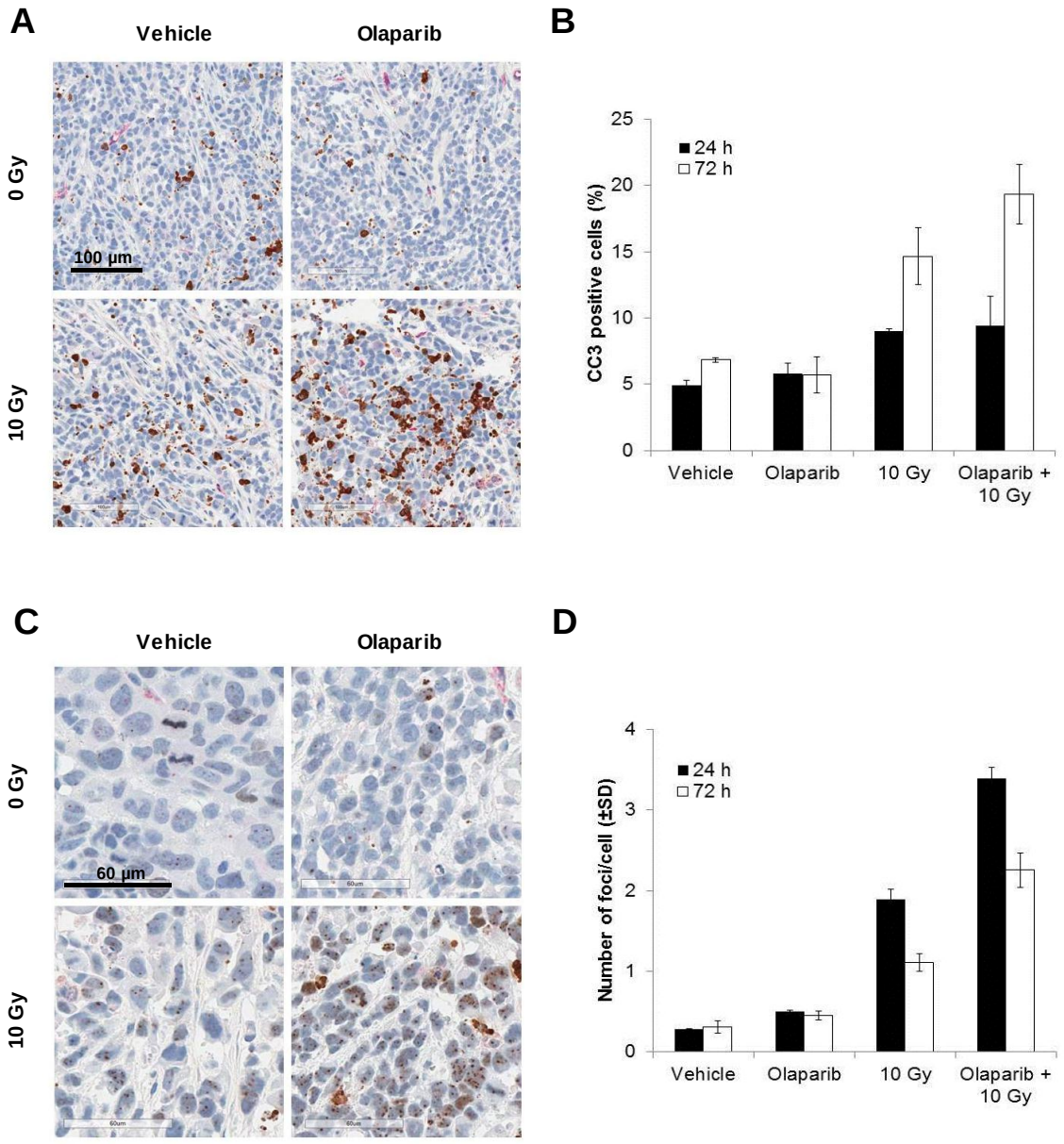

Figure 3.16 Combination treatment of olaparib and radiation increases the apoptotic index and decreases DNA repair in a Calu-6 xenograft model

Histology sections were obtained from Calu-6 xenografts 24 h (3 animals/group) and 72 h (3animals/group) after initiation of treatment. (A) representative CC3 stained images at the 72 h time-point (bar, 100 µm), (B) average CC3 positive cells for each group determined by counting percent positive cells per tumour (bars, SEM; $P = 0.036$ for combination versus radiation treatment alone), (C) representative γH2AX stained images at the 72 h time-point (bar, 60 µm), (D) average number of γH2AX foci per cell determined by counting number of foci/500 cells per tumour (bars, SEM; $P < 0.01$ for combination versus radiation alone).

3.5.2. Proliferation, apoptosis and DNA repair in Calu-3 xenografts

The Ki67 proliferative index varied between tumour samples (27 % - 34 %), but there was no difference between the treatment groups. At the 24 h time-point, CC3 staining of the radiation treated tumours showed similar apoptosis levels to that of the combination treated tumours (Fig 3.17A and B). At the 72 h time-point, the radiation treated and combination treated tumours did not differ significantly from the apoptosis levels at the 24 h time-point. Overall, apoptosis levels were markedly lower compared to apoptosis levels observed in Calu-6 xenografts. As shown in Figure 3.17C and D, at the 24 h time-point, the number of γH2AX foci per cell did not differ significantly between the radiation treated and combination treated tumours. At the 72 h time-point, the number of γH2AX foci per cell had decreased by approximately 50 % in both the radiation and combination treated tumours.

3.5.3. Vasculature and hypoxia in NSCLC xenografts

Histology sections of Calu-3 and Calu-6 xenografts were double-stained for CD31 (a blood vessel marker) and CAIX (carbonic anhydrase IX, a transmembrane protein whose expression is hypoxia-inducible and pH dependent). The tumour oxygenation status can be assessed by either intrinsic (e.g. CAIX and HIF-1α) or extrinsic (e.g. EF5 and pimonidazole) markers of hypoxia. The major drawback of the extrinsic markers is the requirement of an IP injection before tumour sampling. Overall, Calu-3 xenografts appeared well vascularised and no significant CAIX staining was present in any of the tumours (Fig 3.18B). In contrast, substantial areas of hypoxia were present in Calu-6 xenografts (Figure 3.18A). Due to technical difficulties and time limitations, we were unable to quantify the microvessel density of either tumour model.

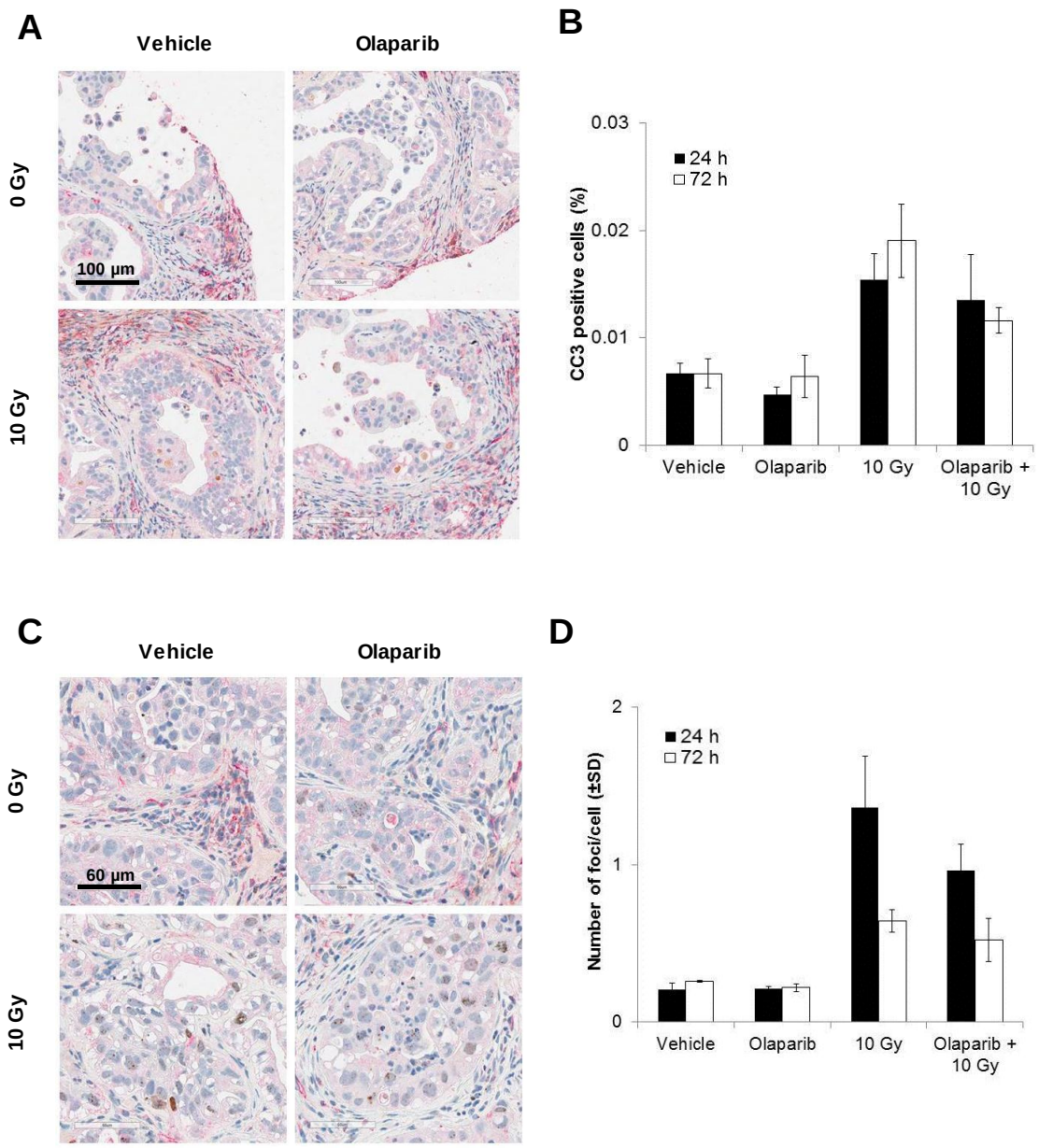

Figure 3.17 Combination of olaparib and radiation therapy is not more beneficial than radiation therapy alone in a Calu-3 xenograft model

Histology sections were obtained from Calu-3 xenografts 24 h (3 animals/group) and 72 h (3 animals/ group) after initiation of treatment. (A) representative CC3 stained images at the 72 h time-point (bar, 100 µm), (B) average CC3 positive cells for each group determined by counting percent positive cells per tumour (bars, SEM), (C) representative γH2AX stained images at the 72 h time-point (bar, 60 µm), (D) average number of γH2AX foci per cell determined by counting number of foci/500 cells per tumour (bars, SEM).

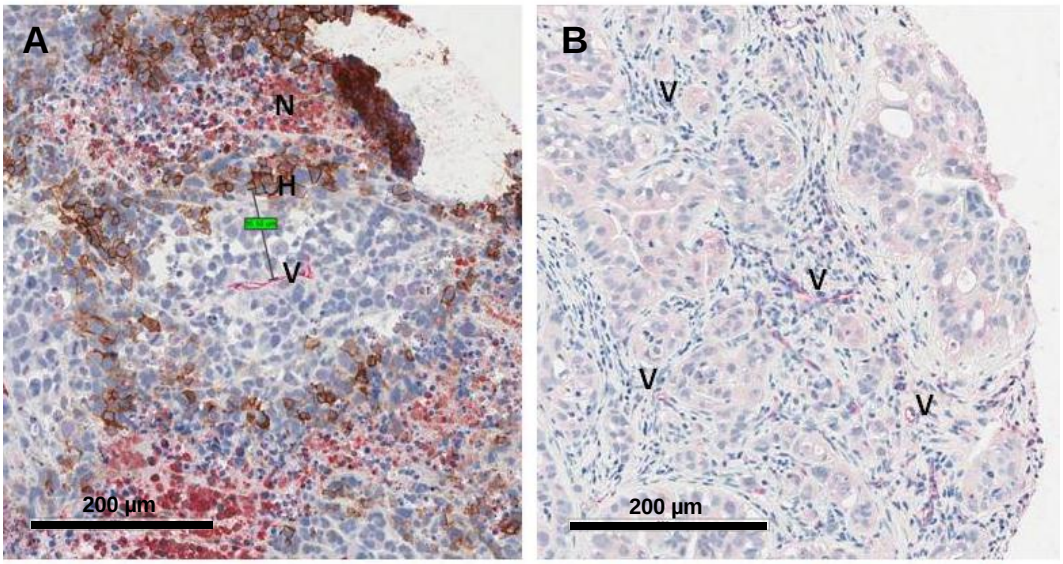

Figure 3.18 Calu-3 xenografts are more vascularised than Calu-6 xenografts

Histology sections were double-stained for CD31 and CAIX. (A) representative image of Calu-6 xenograft with blood vessel (V), hypoxia (H) and necrosis (N). Approximately 100 µm away from blood vessels, a clear band of hypoxia is present, (B) representative image of Calu-3 xenograft (bar, 200 µm).

3.6. Effect of olaparib on vascular perfusion *in vivo*

Olaparib has been shown previously to affect the tumour vasculature *in vivo* using a dorsal window chamber model (Senra, Telfer et al. 2011). To determine whether vasoactive effects can be demonstrated with a more clinically applicable imaging technique, tumour bearing mice were injected twice 22 h apart [vehicle or olaparib (50 mg/kg)]. For each animal, DCE-MRI imaging was performed 2 h before the first and 2 h after the second treatment (Table 2.5). The initial area under the gadodiamide uptake curve was calculated for the first 90 sec for each pre- and post-treatment DCE-MRI (IAUC90 mM.s). For statistical analysis, 50 % (median) values were compared. The average pre-treatment median IAUC90 value of the Calu-3 xenografts was significantly higher compared with the Calu-6 xenografts, indicating that the Calu-3 xenograft is a more vascularised tumour model ($P = 0.04$). No significant differences were present between the pre- and post-treatment median IAUC90 values in either model (Figure 3.19).

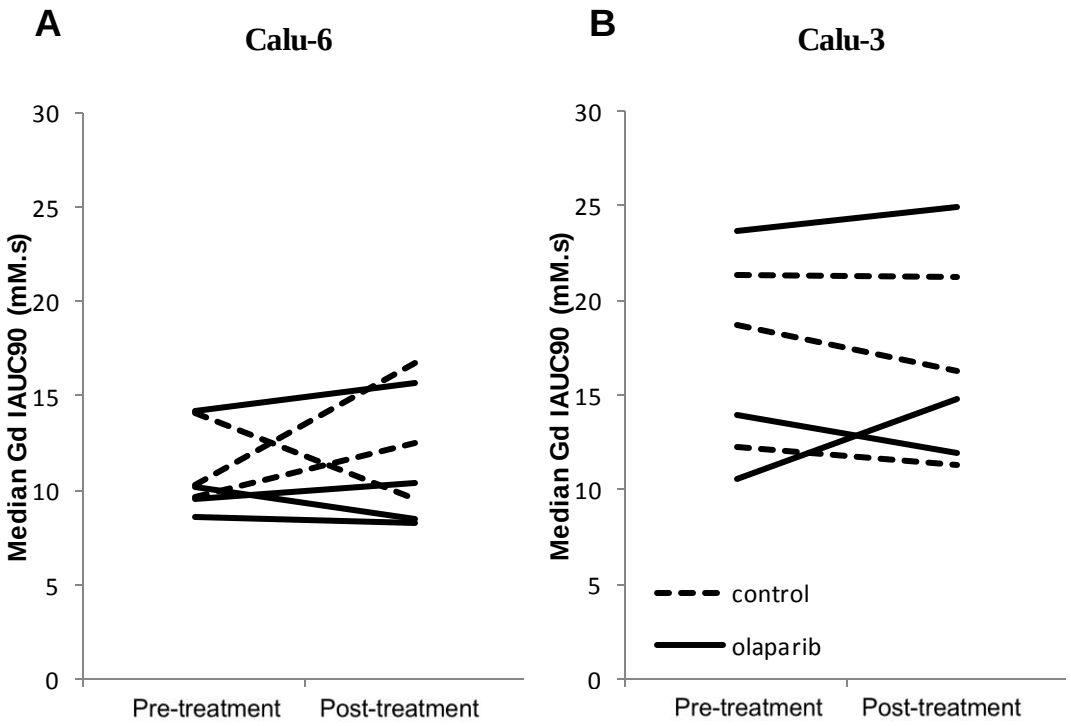

C

Pre IAUC90 (mM.s)	Post IAUC90 (mM.s)
Control Calu-6	
9.61	12.48
10.32	16.69
14.08	9.51
Olaparib Calu-6	
10.15	8.47
8.63	8.29
9.53	10.38
14.22	15.63

D

Pre IAUC90 (mM.s)	Post IAUC90 (mM.s)
Control Calu-3	
12.25	11.28
21.32	21.27
18.73	16.23
Olaparib Calu-3	
10.53	14.79
23.71	24.98
13.95	11.92

Figure 3.19 Olaparib does not alter vascular perfusion in NSCLC models

Tumour bearing mice (3-4 animals per treatment group) were injected twice 22 h apart [vehicle or olaparib (50 mg/kg)]. DCE-MRI imaging was performed 2 h before the first and 2 h after the second treatment. (A and C) pre- and post-treatment median IAUC90 values of Calu-6 xenografts, (B and D) pre- and post-treatment median IAUC90 values of Calu-3 xenografts.

For imaging, we wanted to utilise a clinically relevant parameter. Two MRI primary endpoints (K^{trans} and IAUC) have been recommended for evaluating anti-vascular therapies in the clinic (Leach, Brindle et al. 2005). We chose the IAUC parameter as the primary endpoint in our studies since it does not require curve-fitting, or a prior physiological model, and so is likely to be more robust than K^{trans}, which can be vulnerable to fit failures in highly vascular or poorly perfused tumour regions. Nonetheless, although IUAC reflects blood flow, vascular permeability, and interstitial space, its relationship to underlying physiology has not been defined (Leach, Brindle et al. 2005).

CHAPTER 4

Discussion

4. Discussion

Approximately 50 % of all NSCLC patients receive radiation therapy during the course of their disease, and the quest to enhance the radiation response of these patients is still ongoing. Here, we investigate the potential to increase the radiation response of NSCLC by targeting the PI3K signalling pathway with PDK1 inhibitors and/or targeting DNA repair with the PARP inhibitor olaparib.

First, PDK1 inhibition by BX912 or the highly specific GSK2334470 did not enhance the radiosensitivity of NSCLC cell lines *in vitro*, independently of the *TP53* status of the investigated cells. To confirm the inhibition of the downstream signalling of the PI3K signalling pathway, we assessed the phosphorylation levels of S6 (a downstream target of PDK1). A substantial inhibition of S6 phosphorylation was observed at 1 µM GSK2334470 and above, which is consistent with previous findings (Najafov, Sommer et al. 2011). Najafov and colleagues also reported that GSK2334470 failed to inhibit the phosphorylation of AKT Thr308 under high PI3K signalling levels (e.g. IGF1 stimulation or PTEN deficiency). Surprisingly, GSK2334470 did inhibit the AKT Thr308 phosphorylation under low PI3K signalling levels. They attributed the inability of PDK1 inhibitors to suppress AKT activation by PDK1, to two alternative mechanisms by which AKT can be activated: (1) colocalised PDK1 and AKT bind to PIP3 and (2) AKT Ser473 phosphorylation by mTORC2 followed by PDK1 PIF-pocket interaction (Najafov, Shpiro et al. 2012). Therefore even residual amounts of PDK1 could induce an efficient AKT activation. This is further supported by studies on PTEN-deficient transgenic mice, where despite efficient PDK1 knockdown (> 90 %), the PI3K signalling pathway was modestly

inhibited and no suppression of tumour formation resulting from PTEN loss was observed. Additionally, they showed that AKT and mTOR inhibitors were more potent in suppressing activated PI3K signalling (Ellewood-Yen, Keilhack et al. 2011). AKT inhibition has been reported to radiosensitise tumour cells, including lung cancer (Brognard, Clark et al. 2001; Martelli, Tazzari et al. 2003; Fujiwara, Iwado et al. 2007). However, data from our laboratory using a highly selective allosteric AKT inhibitor, suggested that lung cancer cells were not significantly radiosensitised following AKT inhibition (see appendix). Taken together, our data suggest that inhibiting PDK/AKT may not be an effective combination for further study. Targeting other enzymes in the pathway (e.g. PI3K) may have greater potential for radiosensitisation in NSCLC (Gupta, Cerniglia et al. 2003).

Subsequently, we reported that the PARP inhibitor olaparib radiosensitises a panel of NSCLC cell lines by compromising DNA repair. The combination therapy of olaparib and radiation enhanced the tumour growth delay of a poorly vascularised NSCLC xenograft model by inhibiting the repair of DNA damage and promoting apoptosis. In the present study, we reported that the PAR formation is strongly attenuated at 5 μM olaparib. To confirm that the recruitment of DNA repair machinery would be prevented in the absence of PAR, we compared the γH2AX signal (an indication of DNA DSBs) of irradiated olaparib-treated NSCLC cells and irradiated controls. An t increase in γH2AX signal was observed 2 h after 10 Gy radiation exposure. Twenty-four hours after radiation exposure, the signal intensity had dropped, indicating that the majority of the DNA damage was repaired. When the cells were incubated with olaparib 1 h before radiation exposure, only a small reduction in signal intensity was observed, indicating the repair of DNA damage was compromised.

Similar results were found by immunofluorescent quantification of γH2AX foci formation. Clonogenic survival assays confirmed that olaparib potentiates the cytotoxic effects of radiation in NSCLC cell lines. Although non-tumour cells (NBE1) were radiosensitised to a lesser extent, careful radiotherapy treatment planning should be observed in order to minimise potential normal tissue effects.

We confirmed the *in vitro* findings in the poorly vascularised Calu-6 subcutaneous xenograft model. Olaparib increased the survival probability and potentiated the tumour growth delay induced by radiotherapy while having a minimal effect as monotherapy. To reach a 3-fold increase in tumour volume, tumour growth delay was 2 days for olaparib alone, 13 days for radiation alone and 29 days for the combination treatment. The tumour growth delay we observed in the combination treated xenografts with a single dose of 10 Gy was similar to the tumour growth delay previously reported when olaparib was combined with fractionated (5 x 2 Gy) radiotherapy (Senra, Telfer et al. 2011). This suggests that the benefit of olaparib in combination with radiotherapy is independent of dose fraction. Subsequently, the mechanism of tumour growth delay was investigated. Cleaved caspase 3 staining showed a notable increase in apoptosis in tumours treated with the combination treatment, compared with the controls or either treatment alone, with the combination treated tumours showing 3 times more apoptotic cells compared with controls. Similarly, the combination treated group showed significantly more γH2AX foci per cell, compared with the controls or either treatment alone. No differences in Ki67 staining, a proliferation marker, were observed. Overall, these findings suggest that the mechanism of action includes both decreased DNA repair and increased apoptosis.

In contrast, the well vascularised Calu-3 xenograft model, showed a high intrinsic radiosensitivity and the combination treatment did not enhance the radiation response, compared with radiation alone. As the Calu-3 xenograft response to radiation alone was very significant (causing tumour regression/cytostasis), a combination of olaparib and a lower dose of radiotherapy could be explored to investigate the potential benefit of olaparib addition to lower doses of radiation.

In the Calu-6 cell line, a potent radiosensitisation was observed after olaparib treatment both *in vitro* and *in vivo*, with inhibition of DNA repair as a likely mechanism of action. On the other hand, in the Calu-3 cell line, the *in vitro* olaparib-induced radiosensitisation was not observed *in vivo*. From the results of the *in vivo* γH2AX foci formation experiments, it appears that the DNA DSBs in Calu-3 cells are repaired more quickly than in Calu-6 cells. Previous data from our laboratory showed that 1 h after 10 Gy irradiation of tumour xenografts, the levels of γH2AX foci are similar in Calu-3 and Calu-6 cells. Here, we report that 24 h after radiation exposure, the residual damage is greater in Calu-6 cells than in Calu-3 cells, suggesting a higher level of repair in Calu-3 cells. DNA DSB repair is less effective in hypoxia (Bristow and Hill 2008) and Calu-3 xenografts appear to be more vascularised (as seen with DCE-MRI) and better oxygenated (as seen with CAIX staining) than Calu-6 xenografts, which could in part explain why γH2AX levels decrease more rapidly and more completely in Calu-3 xenografts. Due to technical difficulties and time limitations, we were unable to quantify the microvessel density of either tumour model. Although the existing literature supports our statement regarding the difference in vascularity between the two examined NSCLC xenografts (Smith, Baker et al. 2013), we suggest quantifying the microvessel density in our models, using a microvessel density algorithm.

Clonogenic survival assays showed that the intrinsic radiosensitivity of Calu-3 cells was higher than Calu-6 cells which might also in part explain the higher radiosensitivity of Calu-3 xenografts compared with Calu-6 xenografts. The lack of effect from olaparib addition to radiation *in vivo* was unexpected. It is possible that an effect might have become evident if tumours were allowed to grow for a longer period. Alternatively, the effect of olaparib *in vivo* may be more apparent in situations where DNA repair is already suboptimal (e.g. in hypoxia). Overall, it is clear from our models that the *in vivo* radiosensitivity does not correlate well with residual DNA DSBs (γH2AX staining) or apoptosis (CC3 staining), and therefore these may not be useful as biomarkers of response to radiation (either alone or in combination with olaparib).

Several PARP inhibitors, including olaparib, have been reported with vasoactive characteristics (Calabrese, Almassy et al. 2004; Ali, Telfer et al. 2009; Senra, Telfer et al. 2011). To determine whether these vascular changes could be detected with an imaging system available in the clinic, we investigated the effect of olaparib on *in vivo* vascular perfusion using dynamic contrast enhanced-magnetic resonance imaging. Using this technique, we were not able to observe any differences between the olaparib and vehicle treated xenografts. We hypothesise that the *in vivo* radiosensitising effect seen with olaparib is mainly attributable to inhibited DNA repair. Although vascular effects might also contribute, these effects may not be large enough to be detected by DCE-MRI. Therefore, we suggest it is unlikely that DCE-MRI would be able to detect vascular effects of olaparib in the clinic.

Forthcoming experiments include assessment of the PARP activity in tumour xenografts after IP injection with olaparib, prolonged olaparib treatment after radiation (e.g. 10 days) and confirmation of the efficacy in other NSCLC models (such as the NSCLC cell line A549).

In conclusion, we demonstrated that the potent PARP inhibitor olaparib enhances the radiosensitivity of a poorly vascularised NSCLC xenograft model by decreasing DNA repair and increasing apoptosis. In contrast, a well vascularised NSCLC model was not sensitised by addition of olaparib to the radiation treatment. Recently, a phase I clinical trial was initiated to investigate the radiosensitising effects of olaparib in locally advanced lung cancer patients. Our data suggest that further *in vivo* experiments are warranted to identify the subset of patients that would benefit from olaparib addition to radiation therapy.

CHAPTER 5

Bibliography

5. Bibliography

Albert, J. M., C. Cao, et al. (2007). "Inhibition of poly(ADP-ribose) polymerase enhances cell death and improves tumor growth delay in irradiated lung cancer models." Clin Cancer Res **13**(10): 3033-3042.

Ali, M., B. A. Telfer, et al. (2009). "Vasoactivity of AG014699, a clinically active small molecule inhibitor of poly(ADP-ribose) polymerase: a contributory factor to chemopotentiation in vivo?" Clin Cancer Res **15**(19): 6106-6112.

Bain, J., L. Plater, et al. (2007). "The selectivity of protein kinase inhibitors: a further update." Biochem J **408**(3): 297-315.

Bamford, S., E. Dawson, et al. (2004). "The COSMIC (Catalogue of Somatic Mutations in Cancer) database and website." Br J Cancer **91**(2): 355-358.

Barbera, L., J. Zhang-Salomons, et al. (2003). "Defining the need for radiotherapy for lung cancer in the general population: a criterion-based, benchmarking approach." Med Care **41**(9): 1074-1085.

Bareschino, M. A., C. Schettino, et al. (2011). "Treatment of advanced non small cell lung cancer." J Thorac Dis **3**(2): 122-133.

Billen, D. (1990). "Spontaneous DNA damage and its significance for the "negligible dose" controversy in radiation protection." Radiat Res **124**(2): 242-245.

Boehringer Ingelheim Pharmaceuticals (2013). FDA approves GILOTRIFTM (afatinib) as first-line treatment for metastatic non-small cell lung cancer with common EGFR mutations.

Bristow, R. G. and R. P. Hill (2008). "Hypoxia and metabolism. Hypoxia, DNA repair and genetic instability." Nat Rev Cancer **8**(3): 180-192.

Bradley, D., J.J. Tessier, et al. (2007). "Correlation of MRI biomarkers with tumor necrosis in Hras5 tumor xenograft in athymic rats." Neoplasia **9**(5): 382-391.

Brognard, J., A. S. Clark, et al. (2001). "Akt/protein kinase B is constitutively active in non-small cell lung cancer cells and promotes cellular survival and resistance to chemotherapy and radiation." Cancer Res **61**(10): 3986-3997.

Calabrese, C. R., R. Almassy, et al. (2004). "Anticancer chemosensitization and radiosensitization by the novel poly(ADP-ribose) polymerase-1 inhibitor AG14361." J Natl Cancer Inst **96**(1): 56-67.

Caldecott, K. W. (2003). "XRCC1 and DNA strand break repair." DNA Repair (Amst) **2**(9): 955-969.

Caldecott, K. W., J. D. Tucker, et al. (1995). "Characterization of the XRCC1-DNA ligase III complex in vitro and its absence from mutant hamster cells." Nucleic Acids Res **23**(23): 4836-4843.

Cancer Research UK. (2012). "Lung cancer survival statistics." Retrieved 20/08/2013, from http://www.cancerresearchuk.org/cancer-info/cancerstats/.

Cantley, L. C. (2002). "The phosphoinositide 3-kinase pathway." Science **296**(5573): 1655-1657.

Chalmers, A. J. (2004). "Poly(ADP-ribose) polymerase-1 and ionizing radiation: sensor, signaller and therapeutic target." Clin Oncol (R Coll Radiol) **16**(1): 29-39.

Cockcroft, X. L., K. J. Dillon, et al. (2006). "Phthalazinones 2: Optimisation and synthesis of novel potent inhibitors of poly(ADP-ribose)polymerase." Bioorg Med Chem Lett **16**(4): 1040-1044.

Currie, R. A., K. S. Walker, et al. (1999). "Role of phosphatidylinositol 3,4,5-trisphosphate in regulating the activity and localization of 3-phosphoinositide-dependent protein kinase-1." Biochem J **337 (Pt 3)**: 575-583.

D'Amours, D., S. Desnoyers, et al. (1999). "Poly(ADP-ribosyl)ation reactions in the regulation of nuclear functions." Biochem J **342 (Pt 2)**: 249-268.

Davidovic, L., M. Vodenicharov, et al. (2001). "Importance of poly(ADP-ribose) glycohydrolase in the control of poly(ADP-ribose) metabolism." Exp Cell Res **268**(1): 7-13.

de Murcia, G. and J. Menissier de Murcia (1994). "Poly(ADP-ribose) polymerase: a molecular nick-sensor." Trends Biochem Sci **19**(4): 172-176.

de Murcia, J. M., C. Niedergang, et al. (1997). "Requirement of poly(ADP-ribose) polymerase in recovery from DNA damage in mice and in cells." Proc Natl Acad Sci U S A **94**(14): 7303-7307.

Delaney, C. A., L. Z. Wang, et al. (2000). "Potentiation of temozolomide and topotecan growth inhibition and cytotoxicity by novel poly(adenosine diphosphoribose) polymerase inhibitors in a panel of human tumor cell lines." Clin Cancer Res **6**(7): 2860-2867.

Ding, R. and M. Smulson (1994). "Depletion of nuclear poly(ADP-ribose) polymerase by antisense RNA expression: influences on genomic stability, chromatin organization, and carcinogen cytotoxicity." Cancer Res **54**(17): 4627-4634.

Donawho, C. K., Y. Luo, et al. (2007). "ABT-888, an orally active poly(ADP-ribose) polymerase inhibitor that potentiates DNA-damaging agents in preclinical tumor models." Clin Cancer Res **13**(9): 2728-2737.

Durkacz, B. W., J. Irwin, et al. (1981). "The Effect of Inhibition of (Adp-Ribose)N Biosynthesis on DNA-Repair Assayed by the Nucleoid Technique." European Journal of Biochemistry **121**(1): 65-69.

Erlanson, D. A., J. W. Arndt, et al. (2011). "Discovery of a potent and highly selective PDK1 inhibitor via fragment-based drug discovery." Bioorg Med Chem Lett **21**(10): 3078-3083.

Farmer, H., N. McCabe, et al. (2005). "Targeting the DNA repair defect in BRCA mutant cells as a therapeutic strategy." Nature **434**(7035): 917-921.

Fei, P. and W. S. El-Deiry (2003). "P53 and radiation responses." Oncogene **22**(37): 5774-5783.

Feldman, R. I., J. M. Wu, et al. (2005). "Novel small molecule inhibitors of 3-phosphoinositide-dependent kinase-1." J Biol Chem **280**(20): 19867-19874.

Ferlay, J., H. R. Shin, et al. (2010). "GLOBOCAN 2008 v2.0, Cancer Incidence and Mortality Worldwide: IARC CancerBase No. 10." Retrieved 20/08/2013, from http://globocan.iarc.fr.

Fong, P. C., D. S. Boss, et al. (2009). "Inhibition of poly(ADP-ribose) polymerase in tumors from BRCA mutation carriers." N Engl J Med **361**(2): 123-134.

Fong, P. C., D. S. Boss, et al. (2009). "Inhibition of Poly(ADP-Ribose) Polymerase in Tumors from BRCA Mutation Carriers." New England Journal of Medicine **361**(2): 123-134.

Fujiwara, K., E. Iwado, et al. (2007). "Akt inhibitor shows anticancer and radiosensitizing effects in malignant glioma cells by inducing autophagy." Int J Oncol **31**(4): 753-760.

Goodhead, D. T. (1994). "Initial events in the cellular effects of ionizing radiations: clustered damage in DNA." Int J Radiat Biol **65**(1): 7-17.

Gupta, A. K., G. J. Cerniglia, et al. (2003). "Radiation sensitization of human cancer cells in vivo by inhibiting the activity of PI3K using LY294002." Int J Radiat Oncol Biol Phys **56**(3): 846-853.

Hall, E. J. and A. J. Giaccia (2006). Radiobiology for the radiologist. Philadelphia, Pa. ; London, Lippincott Williams & Wilkins.

Hennessy, B. T., D. L. Smith, et al. (2005). "Exploiting the PI3K/AKT pathway for cancer drug discovery." Nat Rev Drug Discov **4**(12): 988-1004.

Herbst, R. S., J. V. Heymach, et al. (2008). "Lung cancer." N Engl J Med **359**(13): 1367-1380.

Herceg, Z. and Z. Q. Wang (2001). "Functions of poly(ADP-ribose) polymerase (PARP) in DNA repair, genomic integrity and cell death." Mutat Res **477**(1-2): 97-110.

Hoeijmakers, J. H. (2001). "Genome maintenance mechanisms for preventing cancer." Nature **411**(6835): 366-374.

Howlader, N., A. M. Noone, et al. (2013). "SEER Cancer Statistics Review, 1975-2010, National Cancer Institute." Retrieved 20/08/2013, from http://seer.cancer.gov/csr/1975_2010/.

Ihde, D. C. and J. D. Minna (1991). "Non-small cell lung cancer. Part I: Biology, diagnosis, and staging." Curr Probl Cancer **15**(2): 61-104.

Jagtap, P. G., E. Baloglu, et al. (2005). "Discovery of potent poly(ADP-ribose) polymerase-1 inhibitors from the modification of indeno[1,2-c]isoquinolinone." J Med Chem **48**(16): 5100-5103.

Kampf, C., I. Olsson, et al. (2012). "Production of tissue microarrays, immunohistochemistry staining and digitalization within the human protein atlas." J Vis Exp(63).

Konstantinidou, G., E. A. Bey, et al. (2009). "Dual phosphoinositide 3-kinase/mammalian target of rapamycin blockade is an effective radiosensitizing strategy for the treatment of non-small cell lung cancer harboring K-RAS mutations." Cancer Res **69**(19): 7644-7652.

Kortmann, U., J. N. McAlpine, et al. (2011) "Tumor growth inhibition by olaparib in BRCA2 germline-mutated patient-derived ovarian cancer tissue xenografts." Clin Cancer Res **17**(4): 783-791.

Kumareswara R., O. Ludkovski, et al. (2012). "Chronic hypoxia compromises repair of DNA double-strand breaks to drive genetic instability." J Cell Sci 125, 189–199.

Kuzminov, A. (2001). "Single-strand interruptions in replicating chromosomes cause double-strand breaks." Proc Natl Acad Sci U S A **98**(15): 8241-8246.

Lally, B. E., D. Zelterman, et al. (2006). "Postoperative radiotherapy for stage II or III non-small-cell lung cancer using the surveillance, epidemiology, and end results database." J Clin Oncol **24**(19): 2998-3006.

Leach, M.O., K.M.Brindle, et al. (2005). "The assessment of antiangiogenic and antivascular therapies in early-stage clinical trials using magnetic resonance imaging: issues and recommendations." Br J Cancer **92**(9): 1599–1610.

Li, H. F., J. S. Kim, et al. (2009). "Radiation-induced Akt activation modulates radioresistance in human glioblastoma cells." Radiat Oncol **4**: 43.

Liu, S. K., C. Coackley, et al. (2008). "A novel poly(ADP-ribose) polymerase inhibitor, ABT-888, radiosensitizes malignant human cell lines under hypoxia." Radiother Oncol **88**(2): 258-268.

Malvezzi, M., P. Bertuccio, et al. (2013). "European cancer mortality predictions for the year 2013." Ann Oncol **24**(3): 792-800.

Martelli, A. M., P. L. Tazzari, et al. (2003). "A new selective AKT pharmacological inhibitor reduces resistance to chemotherapeutic drugs, TRAIL, all-trans-retinoic acid, and ionizing radiation of human leukemia cells." Leukemia **17**(9): 1794-1805.

Mason, K. A., D. Valdecanas, et al. (2008). "INO-1001, a novel inhibitor of poly(ADP-ribose) polymerase, enhances tumor response to doxorubicin." Invest New Drugs **26**(1): 1-5.

McCabe, N., N. C. Turner, et al. (2006). "Deficiency in the repair of DNA damage by homologous recombination and sensitivity to poly(ADP-ribose) polymerase inhibition." Cancer Res **66**(16): 8109-8115.

McDermott, U., A. J. Iafrate, et al. (2008). "Genomic alterations of anaplastic lymphoma kinase may sensitize tumors to anaplastic lymphoma kinase inhibitors." Cancer Res **68**(9): 3389-3395.

Medina, J. R., C. J. Becker, et al. (2011). "Structure-based design of potent and selective 3-phosphoinositide-dependent kinase-1 (PDK1) inhibitors." J Med Chem **54**(6): 1871-1895.

Miknyoczki, S. J., S. Jones-Bolin, et al. (2003). "Chemopotentiation of temozolomide, irinotecan, and cisplatin activity by CEP-6800, a poly(ADP-ribose) polymerase inhibitor." Mol Cancer Ther **2**(4): 371-382.

Milam, K. M., G. H. Thomas, et al. (1986). "Disturbances in DNA precursor metabolism associated with exposure to an inhibitor of poly(ADP-ribose) synthetase." Exp Cell Res **165**(1): 260-268.

Murphy, S. T., G. Alton, et al. (2011). "Discovery of novel, potent, and selective inhibitors of 3-phosphoinositide-dependent kinase (PDK1)." J Med Chem **54**(24): 8490-8500.

Nagata, Y., A. Takahashi, et al. (2010). "Effect of rapamycin, an mTOR inhibitor, on radiation sensitivity of lung cancer cells having different p53 gene status." Int J Oncol **37**(4): 1001-1010.

Najafov, A., E. M. Sommer, et al. (2011). "Characterization of GSK2334470, a novel and highly specific inhibitor of PDK1." Biochem J **433**(2): 357-369.

Norbury, C. J. and I. D. Hickson (2001). "Cellular responses to DNA damage." Annu Rev Pharmacol Toxicol **41**: 367-401.

Oliver, F. J., G. de la Rubia, et al. (1998). "Importance of poly(ADP-ribose) polymerase and its cleavage in apoptosis. Lesson from an uncleavable mutant." J Biol Chem **273**(50): 33533-33539.

Olsson A., Y. Sheng, et al. (1995). "In vivo tumor measurement of DNA damage, DNA repair and NAD pools as indicators of radiosensitization by metoclopramide." Carcinogenesis **16**(5): 1029-1035.

Powell, C., C. Mikropoulos, et al. (2010). "Pre-clinical and clinical evaluation of PARP inhibitors as tumour-specific radiosensitisers." Cancer Treat Rev **36**(7): 566-575.

Raimondi, C. and M. Falasca (2011). "Targeting PDK1 in cancer." Curr Med Chem **18**(18): 2763-2769.

Rogakou, E. P., C. Boon, et al. (1999). "Megabase chromatin domains involved in DNA double-strand breaks in vivo." J Cell Biol **146**(5): 905-916.

Rothkamm ,K., I. Kruger, et al. (2003). "Pathways of DNA double-strand break repair during the mammalian cell cycle." Mol Cell Biol **23**(16):5706-5715.

Rottenberg, S., J.E. Jaspers, et al. (2008). " High sensitivity of BRCA1-deficient mammary tumors to the PARP inhibitor AZD2281 alone and in combination with platinum drugs." Proc Natl Acad Sci USA **105** (44): 17079-17084.

Saintigny, P. and J. A. Burger (2012). "Recent advances in non-small cell lung cancer biology and clinical management." Discov Med **13**(71): 287-297.

Sandhu, S. K., T. A. Yap, et al. (2010). "Poly(ADP-ribose) polymerase inhibitors in cancer treatment: a clinical perspective." Eur J Cancer **46**(1): 9-20.

Sandler, A., R. Gray, et al. (2006). "Paclitaxel-carboplatin alone or with bevacizumab for non-small-cell lung cancer." N Engl J Med **355**(24): 2542-2550.

Schabel, M. C. and D. L. Parker (2008). "Uncertainty and bias in contrast concentration measurements using spoiled gradient echo pulse sequences." Phys Med Biol **53**(9): 2345-2373.

Senra, J. M., B. A. Telfer, et al. (2011). "Inhibition of PARP-1 by olaparib (AZD2281) increases the radiosensitivity of a lung tumor xenograft." Mol Cancer Ther **10**(10): 1949-1958.

Smith, N. R., D. Baker, et al. (2013). "Tumor Stromal Architecture Can Define the Intrinsic Tumor Response to VEGF-Targeted Therapy." Clin Cancer Res **19**(24): 6943-6956.

Sordella, R., D. W. Bell, et al. (2004). "Gefitinib-sensitizing EGFR mutations in lung cancer activate anti-apoptotic pathways." Science **305**(5687): 1163-1167.

Stead, L. F., S. Berri, et al. (2012). "The transcriptional consequences of somatic amplifications, deletions, and rearrangements in a human lung squamous cell carcinoma." Neoplasia **14**(11): 1075-1086.

Steel, G. G., T. J. McMillan, et al. (1989). "The 5Rs of radiobiology." Int J Radiat Biol **56**(6): 1045-1048.

Tamguney, T., C. Zhang, et al. (2008). "Analysis of 3-phosphoinositide-dependent kinase-1 signaling and function in ES cells." Exp Cell Res **314**(11-12): 2299-2312.

Tapodi, A., B. Debreceni, et al. (2005). "Pivotal role of Akt activation in mitochondrial protection and cell survival by poly(ADP-ribose)polymerase-1 inhibition in oxidative stress." J Biol Chem **280**(42): 35767-35775.

Taylor, A. M., D. G. Harnden, et al. (1975). "Ataxia telangiectasia: a human mutation with abnormal radiation sensitivity." Nature **258**(5534): 427-429.

Thomas, H. D., C. R. Calabrese, et al. (2007). "Preclinical selection of a novel poly(ADP-ribose) polymerase inhibitor for clinical trial." Mol Cancer Ther **6**(3): 945-956.

Thraves, P. J., K. L. Mossman, et al. (1986). "Differential radiosensitization of human tumour cells by 3-aminobenzamide and benzamide: inhibitors of poly(ADP-ribosylation)." Int J Radiat Biol Relat Stud Phys Chem Med **50**(6): 961-972.

Tutt, A., D. Bertwistle, et al. (2001). "Mutation in Brca2 stimulates error-prone homology-directed repair of DNA double-strand breaks occurring between repeated sequences." Embo Journal **20**(17): 4704-4716.

Veuger, S. J., N. J. Curtin, et al. (2003). "Radiosensitization and DNA repair inhibition by the combined use of novel inhibitors of DNA-dependent protein kinase and poly(ADP-ribose) polymerase-1." Cancer Res **63**(18): 6008-6015.

Wang, L., K.A. Mason, et al. (2012). "MK-4827, a PARP-1/-2 inhibitor, stroblgy enhances response of human lung and breast cancer xenografts to radiation." Invest New Drugs **30**(6):2113-2120.

Whitehouse, C. J., R. M. Taylor, et al. (2001). "XRCC1 stimulates human polynucleotide kinase activity at damaged DNA termini and accelerates DNA single-strand break repair." Cell **104**(1): 107-117.

World Health Organization. (2013). "International Clinical Trials Registry Platform." Retrieved 30/09/2013, from http://www.who.int/ictrp/en/.

Yamamoto, H., H. Shigematsu, et al. (2008). "PIK3CA mutations and copy number gains in human lung cancers." Cancer Res **68**(17): 6913-6921.

Yuan, T. L. and L. C. Cantley (2008). "PI3K pathway alterations in cancer: variations on a theme." Oncogene **27**(41): 5497-5510.

Yushkevich, P. A., J. Piven, et al. (2006). "User-guided 3D active contour segmentation of anatomical structures: significantly improved efficiency and reliability." Neuroimage **31**(3): 1116-1128.

Zhang, T., G. B. Cui, et al. (2010). "Inhibition of PI3 kinases enhances the sensitivity of non-small cell lung cancer cells to ionizing radiation." Oncol Rep **24**(6): 1683-1689.

CHAPTER 6

Appendix

6. Appendix

Poster to be presented at the NCRI conference 2013, showing that a highly selective AKT kinase inhibitor does not radiosensitise NSCLC cell lines.

Impact of PDK1 (PDPK1) inhibition on radiation response of non-small cell lung cancer (NSCLC) cell lines

Tom Verbiest, Anika Weber, Sivan Bokobza, Aoife Devery, Yanyan Jiang and Anderson Ryan

Gray Institute for Radiation Oncology and Biology, Department of Oncology, Oxford University, Old Road Campus Research Building, Headington, Oxford, OX3 7DQ

Introduction

The PI3K/PDK1/AKT signalling pathway regulates cell metabolism, proliferation and survival and is dysregulated/activated in the majority of human cancers. In lung cancer in particular, high pathway activation levels have been associated with resistance to therapy and poor prognosis. PDK1 functions as a pivotal kinase in this pathway, phosphorylating and activating several downstream kinases including AKT and p70/p90 ribosomal protein S6 kinases.

Therefore, PDK1 represents a promising target for cancer therapy either alone or in combination with established therapies, including ionising radiation.

PI3K/PDK1/AKT signalling pathway

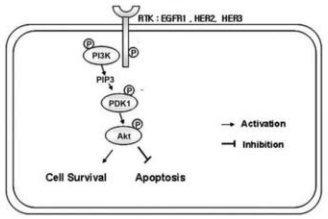

Modified from Kwon et al, Chembiochem. 11 (4), 2010

PDK1 inhibitors decrease cell proliferation

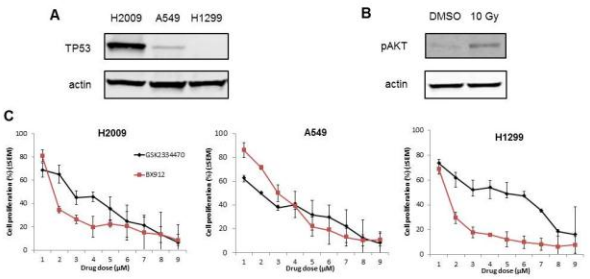

NSCLC cell lines (A549, H1299 and H2009) differing in TP53 status (wild-type, null and mutant, respectively) were studied (A). Irradiation of NSCLC cells leads to an upregulation of pAKT levels, thereby increasing anti-apoptotic signalling (B). IC50 values for growth inhibition were determined using a resazurin based proliferation assay (average IC50 values for the PDK1 inhibitors BX-912 and GSK2334470, 2.0 and 2.6 μM, respectively) (C)

GSK2334470 inhibits downstream signalling

A 0.2 μM concentration of GSK2334470 partially inhibits phosphorylation of S6K. Complete inhibition is observed at 1 μM GSK2334470 and above.

Clonogenic survival following combination of irradiation and PDK1 inhibition

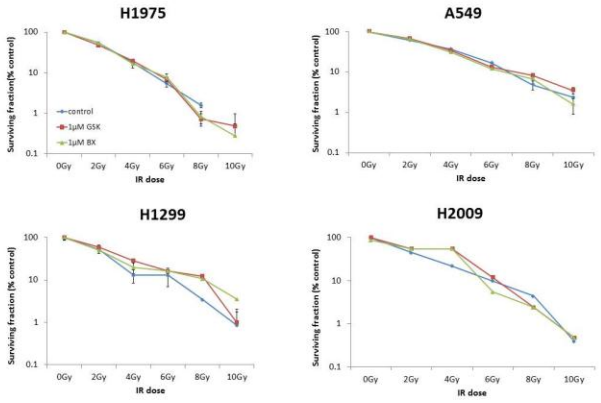

Combination of irradiation with PDK1 inhibitors does not lead to radio-sensitisation in clonogenic survival assays, independently of the TP53 status.

Clonogenic survival following combination of irradiation and AKT inhibition

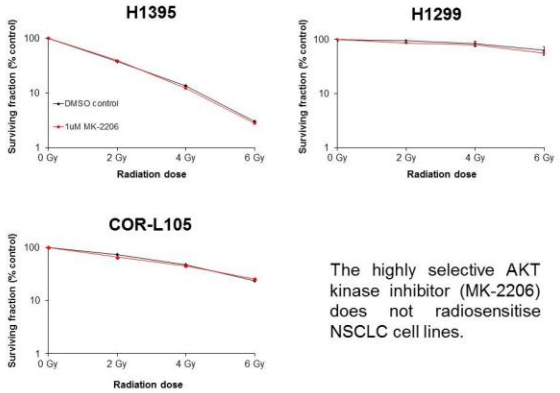

The highly selective AKT kinase inhibitor (MK-2206) does not radiosensitise NSCLC cell lines.

Conclusion

We show that neither PDK1 nor AKT inhibition enhanced radiosensitivity of NSCLC cell lines in vitro. However, inhibiting other enzymes in the pathway (e.g. PI3K) may have greater potential for radiosensitisation in non-small cell lung cancer.